DETERMINATION AND MODELING OF THE INTERACTION BETWEEN ARSENIC AND SILICON INTERSTITIALS IN SILICON

By

RICHARD E. BRINDOS

A DISSERTATION PRESENTED TO THE GRADUATE SCHOOL
OF THE UNIVERSITY OF FLORIDA IN PARTIAL FULFILLMENT
OF THE REQUIREMENTS FOR THE DEGREE OF
DOCTOR OF PHILOSOPHY

UNIVERSITY OF FLORIDA
2001

This work is dedicated to the people who had faith in me to complete it.

ACKNOWLEDGMENTS

I would like to first acknowledge my research advisor, Dr. Kevin S. Jones for giving me the chance to study and to succeed at the University of Florida. Dr. Jones made the experience interesting and fun and provided the necessary funding for completion of my projects. I would also like to acknowledge Dr. Mark E. Law for his help with the experimental and modeling efforts in this dissertation and all of the Gator sports talks throughout the last 5 years. I further acknowledge Guna Selvaduray at San Jose State University for giving me the courage and motivation to apply for graduate schools and the continual encouragement to complete my journey into doctor-hood. I would also like to thank the rest of the committee, Dr. Paul Holloway, Dr. Cammy Abernathy, Dr. Kenneth O and Fred Stevie for serving on my committee. I express additional thanks to Fred Stevie for increasing my knowledge and interest in SIMS and Agere Systems (Formerly Lucent Tech.). Without Fred it would have been impossible to get all the SIMS information necessary for this project and others. I also extend special thanks to the administrative assistants (Cindy, Carrie, Michelle, Lauren and Kelly) who have gone through our group, throughout my 5 years, for putting up with me and my rudeness. I

want to thank the industrial folks who made my two internships possible and successful; Bob Ogle and Emi Ishida from AMD; and from Bell Labs-Lucent Technologies, Conor Rafferty, Hong-Ha Vuong, Tony Fiory, Hans Gossman, George Celler, Janet Benton, John Grazul, Ken Short and the party room (Vinnie Venezia, Lourdes Pelaz, Ramki Kalyanaraman, Peter O'Sullivan, Emiliano Rubio, Jacques Dalla Torre). I would also like to acknowledge the industry sponsors from Intel: Paul Packan, Steve Cea and Hal Kennel, who provided research and made all conferences and contact reviews pleasant and memorable. I also thank Eb Andideh from Intel for the growing of the boron spike material.

I would like to extend a very special thanks to Jamie Rhodes and Jay Lewis for being two of the best roommates a guy could have and for putting up with the fur of my cat, Whitey. They are probably still getting the hair out. I extend special thanks to the members of the cabbage organization for their impeccable sports and beer drinking abilities. I never got to win that T-shirt but I had a great deal of fun trying.

I thank all of the SWAMP members past and present for sometimes intellectual conversation, but mostly not. I would like to acknowledge the lunch group of Patrick, Ibo, Chad and Luba for all of the spectacular lunches at Shands Hospital. I thank Aaron Lilak for the use of his carpet steam cleaner and all of the stock-tip advice. I also thank Sushil Bharatan

for his initial research directions and the mountain bike rides (which I haven't gone on since). I would also like to acknowledge Hernan Rueda for all the soccer wounds. I thank Wish for all the TEM advice and research directions.

I thank all the Gator sports coaches for providing championship-winning teams. I give special thanks to Steve Spurrier and Billy Donovan for providing truly great football and basketball teams that were exciting to watch. I would like to acknowledge Ananth Naman for making football tickets a top priority for me to receive upon first arrival. I would also like to thank everyone who was associated with the Salty Dog. This includes Pam, Chuck and the rest of the gang, thank you for everything.

I would like to finally acknowledge the people most responsible for my ability to complete this work. I thank my parents, Helen Rachfal and Raymond Brindos, for their love and financial support. I thank my dad for the wonderful Volkswagen Jetta and for all of the advice on how to fix it. I thank my mom for always being there when needed and for continuing to call weekly throughout my tenure. I also thank my brother for his love and support of my venture. Finally I give thank to my significant other, Monica Taylor, for her patience in the final leg of this journey and for being able to start our ADULT life together. I give thanks again to all. I apologize to and thank all those I left out.

TABLE OF CONTENTS

LIST OF TABLES

LIST OF FIGURES

Abstract of Dissertation Presented to the Graduate School
of the University of Florida in Partial Fulfillment of the
Requirements for the Degree of Doctor of Philosophy

DETERMINATION AND MODELING OF THE INTERACTION BETWEEN ARSENIC AND SILICON INTERSTITIALS IN SILICON

By

Richard E. Brindos

May 2001

Chairman: Dr. Kevin S. Jones
Major Department: Department of Materials Science and Engineering

Arsenic has evolved as the premier dopant for N^+ source and drain structures in current generation processors. To further use arsenic in future devices, research is needed on the transient enhanced diffusion and activation properties. Until now, researchers have concentrated on higher dose arsenic implants. The results from the higher dose implants become difficult to interpret because of effects from implant damage, solubility, and cluster formation. The goal of this research is to use lower arsenic concentrations to determine the basic interaction between arsenic atoms and silicon interstitials. The arsenic-silicon interaction is then

expanded to include the high-dose effects. Arsenic wells of varying concentrations were formulated and silicon implants known to cause {311} defects were added. The structures were then annealed and the nucleation, growth and dissolution of the {311} defects were monitored. Arsenic had a distinct effect on the nucleation but little to no effect on the dissolution. As the arsenic concentration increased, the number of interstitials in the defects at time zero decreased. The same decrease was realized at each temperature studied. The results show that arsenic is pairing with interstitials during the initial stages of the annealing cycle. The pair formation decreases the interstitial population and with fewer interstitials present, fewer defects are able to nucleate. This result also leads to a smaller number of trapped interstitials in {311}'s at higher arsenic concentrations. Using Florida's Object Oriented Process Simulator (FLOOPS) and a simple pair model the experiment was modeled and the binding energy between an arsenic atom and an interstitial was determined to be 0.95 eV.

Boron marker layers were used to monitor the release of interstitials from an arsenic-implanted region. It was found that at the initial stages of annealing, the enhanced motion of the boron marker layer was reduced in comparison to a control wafer with only a silicon implant.

It was also determined that an enhanced diffusion was seen in the arsenic only samples because of an injection of interstitials from cluster formations.

CHAPTER 1
INTRODUCTION

1.1 Motivation and Objective

To comply with the speed and power demands of today's computers, transistor performance must continually increase. A schematic diagram of a typical CMOS transistor used in current generation microprocessors is featured in Figure 1.1. Referring to this figure, the terms used to describe a transistor can be defined. The SDE is the source/drain extension, which is a shallow diffusion that connects the channel or metallurgical spacing with the deep source and drain. The overlap is the distance the SDE extends under the gate and the metallurgical spacing is the channel between the SDEs of the source and drain, where the electron flow is regulated. The junction depth refers to the depth of the SDEs after diffusion.

Gate length, gate dielectric thickness, and junction depths are the primary parameters that control transistor performance. In Figure 1.2, the Semiconductor Industry Association (SIA) roadmap shows that junction depths and gate lengths will continue to decrease in the years to

come.[1] In order to continue this downward trend it becomes increasingly important to understand and control dopant diffusion in silicon.

The manufacturing of shallow junctions mandates the introduction and activation of dopants such that a minimal amount of diffusion occurs. The primary method used to introduce dopants is ion implantation. Activation is achieved through subsequent annealing steps.[2] Ion implantation is known to cause large amounts of lattice damage that must be annealed out in order to restore device performance.[3] During this annealing step, a large supersaturation of point defects is available to enhance the diffusivity of dopants in the area of the implanted region. In some instances the equilibrium diffusivities of the dopants can be increased by three orders of magnitude or more, thereby driving the junction depths to unacceptable values. The enhancement lasts only a short time until the local concentration of point defects returns to the equilibrium value and equilibrium diffusivities are restored. Therefore, the enhanced diffusion is transient in nature and is known as transient enhanced diffusion or TED.

Of the dopants used in today's transistors, arsenic has emerged as the most common n-type dopant. Like other dopants, implanted arsenic in silicon has been shown to exhibit TED. Many studies have concentrated on arsenic TED and the fundamentals associated with it.[4-19] These

studies, however, have concentrated on arsenic concentrations near or above the solid solubility limit and most of the focus of these studies is on electrical activation. Results from these studies often become difficult to interpret because they contain effects from solid-phase epitaxial regrowth, arsenic precipitation, implant damage, and the formation of dislocations. The goal of this work is to take an extensive look at the more fundamental issue of how arsenic and silicon interstitials interact and to provide a model of their behavior.

1.2 Ion Implantation and Defect Generation

1.2.1 Ion Implantation

The ability to change the conduction properties of a semiconductor is the main attribute that makes semiconductors useful for electronic devices. The way to change the conduction properties is to introduce elements, known as dopants, into the semiconductor material such that a high number of charge carriers are generated. This procedure of introducing dopants can be accomplished in a variety of ways. Whichever method is used to introduce dopants must be controllable, reproducible, and free from undesirable side effects. In the past, dopants were introduced by indiffusion. Dopants were diffused in from a surface source such as a doped glass or by holding a constant atmosphere of a dopant-

containing gas over the surface. These were viable methods. However, the amount of dopant able to be introduced was limited by solid solubility and it became difficult to incorporate a sufficient amount of dopant. It was also difficult to laterally diffuse the dopant under surface structures such as gate stacks. Because diffusion from solid sources doesn't supply all the necessary parameters, the technique of ion implantation was developed.[2,20-22]

During ion implantation, a liquid or solid source containing the desired dopant material is heated and emits vapors of the dopant atoms. A cloud of electrons emitted by a heated filament then ionizes the atoms. The ions then pass by an analyzing magnet and unwanted species are filtered out. Correctly filtered ions are then accelerated toward a silicon target and rastered over the surface. A schematic diagram of a typical ion implanter is shown in Figure 1.3.

Monitoring the ion current can control the dopant dose and adjusting the ion acceleration energy can control the average depth of the ions. Ion implantation therefore satisfies the needed parameters for a general doping process. The main disadvantage is the damage done to the silicon lattice due to ion collisions. This damage may be removed by subsequent heat treatments.

1.2.2 Implanted Ions

As energetic ions penetrate a solid target material, they lose energy because of collisions with atomic nuclei and electrons in the target material and the ions eventually come to rest. The ions are stopped in a solid by two processes; nuclear and electronic stopping. These processes are shown in Figure 1.4.

The dominant stopping mechanism depends on the atomic weight and implant energy of the implanted species. At lower energies, a process of nuclear stopping stops ions, while at higher energies ions come to rest by the process of electronic stopping.[23,24] The stopping power of the target is the loss of energy per unit distance, $-dE/ds$, which is defined as

$$\frac{-dE}{ds} = N\left[S_e(E) + S_N(E)\right] \tag{1.1}$$

where, E is the ion energy, s is the coordinate along the path whose direction changes as a result of binary nuclear collisions, N is the density of atoms in the target material, S_e is the electronic stopping power and S_N is the nuclear stopping power. The total distance that an ion travels in a solid is known as the range, and is defined as,

$$R = \int ds = \frac{1}{N}\int_0^E \frac{dE}{S_e(E) + S_N(E)} \tag{1.2}$$

Equation 1.1 was reformulated by Lindhard *et al.*[25](LSS theory) for implantation into amorphous material in terms of the reduced parameters, ε and ρ as,

$$\rho = \frac{RNM_1M_2 4\pi a^2}{M_1 + M_2} \tag{1.3}$$

and,

$$\varepsilon = \frac{E_0 a M_2}{Z_1 Z_2 q^2 \left(M_1 + M_2\right)} \tag{1.4}$$

where, M_1 and Z_1 are the mass and atomic number of the incident ion, respectively; M_2 and Z_2 are the mass and atomic number of the target atoms, respectively; N is the number of atoms per unit volume; and a is the screening length, equal to

$$a = \frac{0.88 a_0}{(Z_1^{1/3} + Z_2^{2/3})^{1/2}} \tag{1.5}$$

where a_o is the Bohr radius. (Calculations for ε and ρ can be found in the paper by Lindhard *et al.*[25]). With Equation 1.3 the value of ρ can be converted to the projected range, R_p, which is the average depth below the surface an ion penetrates, using the expression

$$R_p \cong \frac{R}{1+\left(\frac{M_2}{3M_1}\right)} \tag{1.6}$$

Assuming that the depth profile of the implanted ions in amorphous materials could be described by a symmetrical Gaussian curve, then the ion concentration, n, as a function of depth, x, is given by

$$n(x) = \frac{\phi}{\sqrt{2\pi}\Delta R_p} \exp\left[\frac{-(x-R_p)^2}{2\Delta R_p^2}\right] \tag{1.7}$$

where ϕ is the ion dose in cm^{-2}, x is the junction depth, R_p is the projected range, and ΔR_p is the projected straggle. The standard deviation of the Gaussian distribution ΔR_p is given by

$$\Delta R_p = \frac{2R_p}{3}\left[\frac{\sqrt{M_1 M_2}}{M_1 + M_2}\right] \tag{1.8}$$

The peak concentration occurs when $x=R_p$, which leads to

$$n_{max}(R_p) = \frac{\phi}{\sqrt{2\pi}\Delta R_p} = \frac{0.4\phi}{\Delta R_p} \tag{1.9}.$$

For a given implant the predominantly desired values are the projected range and projected straggle. These parameters are detailed schematically in Figure 1.5. The projected range and projected straggle for boron, phosphorous, and arsenic in silicon and silicon dioxide (SiO_2) for various implant energies can be found in Smith *et al.*[26]

1.3 Implant Damage Characteristics

1.3.1 Ion Collisions

As stated in the previous section, energetic ions are involved in several collisions with lattice atoms before coming to rest in the target material. A collision of ~15 eV is all that is needed to knock a silicon host atom from a lattice site.[21] If adequate energy is transferred in the first collision the displaced atom may collide with other atoms to cause more displacements and collisions. The process continues until the energy of the collisions drops below the lattice displacement energy. Such a process results in a collision cascade.

The damage path created will depend on the relative masses between the dopant atom and the lattice atoms. Figure 1.6 shows a schematic of the lattice disorder that may be created for both light and heavy ions and with enough collision cascades the formation of an amorphous layer will result.[22] An amorphous layer is defined as a layer that exhibits no long-range order. A light ion transfers small amounts of energy during each collision and with a small enough transfer, few additional displacements are created. In the case of a heavy ion, the energy transfer is enough to cause additional collisions. The range of the ions is generally small since the energy transfer is mostly by nuclear

stopping. The small range and nuclear collisions create localized pockets of damage regions. When the dose of the implanted ions is increased to a high enough point, the damage regions begin to overlap and an amorphous region results.[21]

1.3.2 Implantation Related Defects

Ion implantation induced damage to the silicon lattice that must be corrected so that the implanted dopants become electrically active. Upon annealing, the energetically favorable position for an excess ion may not be a lattice site. It is possible that the excess ions cluster together to form extended defects that are more energetically favorable positions for ions to occupy. The type of defect that forms depends on the conditions of the implant (energy, dose, temperature, etc.) and the post-implantation annealing conditions. In order to separate the different types of damage, Jones *et al.*[27] formulated a classification system in which the various types of defects were separated according to the type of damage from which they originated.

Type I damage is formed when the implant conditions are below that of amorphization. In this case point defects cluster around the projected range of the implant where the supersaturation is the highest. Upon annealing, {311} defects or dislocation loops will form due to the clustering of these point defects. Type II damage, also known as end-of-

range (EOR) damage, forms if the implant dose is high enough to cause amorphization. Upon annealing, EOR damage will manifest itself as dislocation loops that form just below the amorphous/crystalline interface. Type III damage results from the regrowth of the amorphous layer and generates several types of defects such as hairpins or microtwins. These types of defects do not seem to affect the diffusivity of dopants, but they can act as gettering sites for impurities such as carbon or oxygen. Type IV damage occurs when buried amorphous layers are created. During regrowth, the regrowing amorphous layer and crystalline layers meet and "clamshell" or "zipper" defects are generated. Type V damage forms when the implant is of a sufficient concentration to reach the solid solubility limit of the dopant in silicon. Upon annealing, precipitates of the impurity atom can form. This type of damage is commonly found in arsenic implanted samples. If the pathway for the formation of this precipitate is through an arsenic-vacancy cluster, then the formation can generate high levels of vacancies which, in turn, can lead to the dissolution of dislocation loops (however, this has never been proven). Type I and II damage are the relevant defect classifications in the portion of this work that involves extended defects. In other portions of this work, implants of arsenic will be chosen carefully such that Type V defects are avoided.

1.4 Point Defect Diffusion

In early devices, critical dimensions were large enough that the amount of diffusion was not a significant factor. However, with the scaling of devices to smaller dimensions, designers are forced to reevaluate the amount of diffusion after annealing. This is complicated due to implant-induced defects that may cause the equilibrium diffusion to be enhanced.

Point defects such as interstitials and vacancies, created during the implant process, are known to cause several problems during processing. For instance, interstitials released by extended defects have been shown to enhance diffusivities of dopants and decrease the activation percentage.[28-31] The main focus of this work is to establish how interstitials interact with arsenic atoms. This information will provide valuable insight in eliminating problems such as TED and low activation in arsenic implanted regions.

1.4.2 Point Defect Diffusion Model

Ion implantation damage is removed through an annealing process. Annealing causes dopants to redistribute in the silicon lattice through the process of diffusion. In early diffusion studies, the diffusivity of impurities was modeled using an Arrhenius equation of the form

$$D(T) = D_0 \exp\left(\frac{E_a}{kT}\right), \tag{1.10}$$

where, D is the diffusion coefficient, D_0 is a temperature-independent pre-exponential, E_a is the activation energy for the diffusion of the impurity, k is Boltzmanns constant, and T is the temperature. The magnitude of the diffusion coefficient, D, indicates the rate at which atoms or impurities diffuse. This equation, however, only describes the influence of temperature on the diffusion of an impurity and has no terms for the mechanisms responsible for the diffusion in silicon.

In silicon, dopant atoms are known to diffuse through interactions with silicon self-interstitials and vacancies.[29] Equation 1.10 does not take this into account and therefore is an unreliable model for dopant diffusion in silicon. In lieu of this, a more complicated model for dopant diffusion in silicon must be constructed.

Dopants diffuse in silicon by combining with either an interstitial or vacancy.[29] The diffusion of a dopant, A, must then be made up of the sum of the diffusion mechanisms or

$$D_A = D_{AI} + D_{AV} \tag{1.11}$$

where, D_{AI} and D_{AV} are the interstitial and vacancy components for the dopant diffusion. If D_A is defined as the dopant diffusion under

nonequilibrium conditions, then D_A^* is the intrinsic diffusion under equilibrium conditions. Dividing Equation 1.11 through by D_A^* leads to

$$\frac{D_A}{D_A^*} = \frac{D_{AI}}{D_A^*} + \frac{D_{AV}}{D_A^*} \tag{1.12}$$

To account for the fraction of diffusion due to interstitials and vacancies, Equation 1.12 can be rewritten as

$$\frac{D_A}{D_A^*} = \frac{D_{AI}^*}{D_{AI}^*}\frac{D_{AI}}{D_A^*} + \frac{D_{AV}^*}{D_{AV}^*}\frac{D_{AV}}{D_A^*} \tag{1.13}$$

The ratio D_{AX}^*/D_A^* (X signifies an interstitial or vacancy) is the fraction of diffusion that occurs through an interstitial or vacancy mechanism. D_{AX}^*/D_A^* can be defined as f_{AX} and because the interstitials and vacancies are the only mechanisms through which dopant diffusion can happen, then

$$f_{AI} + f_{AV} = 1 \tag{1.14}$$

Using this definition, Equation 1.15 can be rewritten as

$$\frac{D_A}{D_A^*} = f_{AI}\frac{D_{AI}}{D_{AI}^*} + (1 - f_{AI})\frac{D_{AV}}{D_{AV}^*} \tag{1.15}$$

D_{AI}/D_{AI}^* and D_{AV}/D_{AV}^* are proportional to the relative concentrations of interstitials, C_I/C_I^*, and vacancies, C_V/C_V^*, and Equation 1.15 can be written in its final form as

$$\frac{D_A}{D_A^*} = f_{AI}\frac{C_I}{C_I^*} + (1 - f_{AI})\frac{C_V}{C_V^*} \tag{1.16}$$

Equation 1.16 shows how point defect concentrations and dopant diffusion are related and shows that by changing the defect concentrations the dopant diffusivities can be adjusted. The important point of this development is that to fully understand dopant diffusion in silicon, it is critical to have an understanding of how the point defect concentrations are affected by different processing steps.

The type of point defects that dominate the diffusion process determines the type of diffusion mechanism, vacancy, interstitial or interstitialcy. In the vacancy mechanism, the substitutional dopant atom migrates through the lattice by moving on to an adjacent lattice site that is vacant. In the interstitial mechanism, the dopant atom is kicked out of a lattice site by a silicon self-interstitial and migrates through the interstices as a dopant interstitial until it returns to a lattice site as a substitutional atom. In the interstitialcy mechanism, the silicon self-interstitial and the dopant atom form a diffusion pair.[29] These processes are shown in Figure 1.7. There is generally no distinction made between the interstitial and interstitialcy mechanisms because they cannot be differentiated from each other.

Studies have been done to determine what fraction of dopant diffusion is interstitial and what fraction is vacancy, for a variety of common dopants. It is generally agreed that boron and phosphorus are

pure interstitial diffusers and therefore, $f_{AI} \approx 1$.[29] On the other hand, antimony has been shown to exhibit pure vacancy diffusion with $f_{AV} \approx 1$.[29] It has also been shown that arsenic exhibits both interstitial and vacancy diffusion with $f_{AI} \approx 0.5$.[29]

Dopants that exhibit pure interstitial or vacancy diffusion can be used as effective marker layers for studying the release of point defects in silicon. Buried marker layers of boron or antimony can lead to essential data on the release of interstitials or vacancies from a specific area of interest. A discussion of how this is accomplished is presented in a future chapter.

1.4.3 Transient Enhanced Diffusion

As device dimensions continue to shrink, source and drain regions become closer together, causing unwanted interactions. Under equilibrium diffusion, annealing should cause minimal motion in the source and drain profiles. However, the ion implantation process introduces interstitials and vacancies that lead to more motion of the profiles than is predicted by equilibrium diffusion. Studies of the enhanced diffusion have shown that the diffusion enhancement decays back to the equilibrium diffusion value over time, therefore the enhancement is transient in nature and classified as transient enhanced diffusion or TED.[29,31-34] If the

dimensions of the device are such that little diffusion is warranted, then the extra diffusion cannot be tolerated. In recent years many research groups have dedicated their studies to the relationship between TED and implant-related defects to understand and control the effects of enhanced diffusion.[28-31,33-38]

The exact nature of TED has been thoroughly studied and debated among many researchers without a general consensus. Some believe that TED is due to the dissolution of extended defects, others feel sub-microscopic clusters are responsible, and a portion feel that a combination of clusters and extended defects are the cause.[32,39-41] Eaglesham *et al.*[39] compared the dissolution of extended defects with the enhanced motion of boron marker layers. It was concluded that the transient duration of TED, and thus the reaction rate constant, increased very rapidly with increasing temperature. By correlating the number of interstitials released during {311} dissolution with the TED duration, they found that the {311}'s could account for the entire enhancement in diffusion rates in the temperature regime 670 to 815°C. Cowern *et al.*[42] did a study of the interaction between interstitials and {311} defects and found two distinct periods of enhancement. The initial period was due to silicon interstitials created by collisions during the implant. The interstitials would either enhance diffusion for low dose implants or drive

the nucleation of {311}'s at higher damage densities. The later period of enhancement was a much slower diffusion transient that was similar to the mechanism described by Eaglesham *et al.*[39] Zhang *et al.*[41] came upon conditions where no defects formed but TED was still present. From this they implied that there may be more than one source of interstitials available for TED. Liu *et al.*[40] found that {311} defects could not account for all of the excess interstitials and suggested that a combination of {311} and cluster dissolution drive TED simultaneously.

Recent work by Cowern *et al.*[36] has shown that there is a nucleation threshold for {311} defects. Therefore, if a sub-microscopic dopant interstitial cluster it might be possible to trap enough interstitials in the clusters to avoid the formation of extended defects. Upon annealing, the clusters may break up and release the interstitials causing enhanced diffusion. Boron, phosphorus, and arsenic have all been shown to exhibit cluster formations that affect the formation of extended defects.[37,43-46]

1.5 Precipitation and Clustering

In the development of new device structures the electrically active fraction of dopants is an important quantity. Through many experiments it is known that above a certain concentration dopants become

electrically inactive.[29,46-51] The concentration of atoms that can become electrically active at a given temperature is generally controlled by the solubility limit. The solubility limit is given by the concentration of dopants that will dissolve substitutionally in the silicon matrix at a given temperature. Concentrations above this level will lead to precipitation of a second phase in the matrix. Precipitation related defects have been considered to be responsible for most of the electrical inactivity in boron, phosphorus, and to some extent antimony.[29]

Like other dopants, arsenic exhibits precipitation if a high enough concentration is obtained. However, electrical inactivity starts well before the solubility limit for formation of a macroscopic second phase is reached. Theories of clustering have been proposed to account for the electrical inactivity, where multiple arsenic atoms form some new configuration with an interstitial or vacancy, which is electrically inactive at room temperature. The difference between precipitates and clusters is that precipitates are a macroscopic second phase that may contain thousands of dopant atoms where the size distribution is a function of the dopant concentration above the solubility limit and the thermal treatment that follows. Clusters, on the other, hand are composed of a few dopant atoms in specific configurations and their formation may be enhanced by excess silicon interstitials. Clusters exist in equilibrium with

isolated dopant atoms just as *AX* defects coexist with an isolated *A*, where precipitates are regions of the crystal that have formed a second phase of the solute and solvent constituents. Dopant will eventually precipitate at high enough concentrations in silicon.

1.6 Arsenic Background

1.6.1 Arsenic Overview

Arsenic is the most common n-type dopant used in silicon based microelectronic device fabrication. High Mass, high solubility, high electrical activation, and low diffusivity are all properties that make arsenic an attractive dopant to the device industry. Although arsenic displays all these desired qualities, transient enhanced diffusion (TED) and electrical activation are still concerns.

TED and electrical activation studies of arsenic implanted samples have lead to the conclusion that there is both an electrical and solid solubility limit associated with arsenic. From this conclusion, it is realized that there are distinct regimes of concentration when dealing with arsenic in terms of TED, activation, and point defects.

At low concentrations (below electrical solubility limit), but above amorphization, TED is dominated by end of range damage and surface

effects. Increasing the arsenic concentration above the electrical solubility limit, leads to arsenic clustering at which point deactivation of the arsenic begins. The clustering reaction is believed to lead to interstitial injection through the reaction $As_nSi \Leftrightarrow As_nV + I$.[50,51] It has been shown that if the interstitial injection reaches a sufficient level then the formation of dislocation loops is possible.[52,53] As the arsenic concentration increases further and the physical solid solubility limit is reached, a monoclinic AsSi phase forms.[16] It has been suggested that the formation of the AsSi phase injects vacancies and causes the dissolution of dislocation loops.[54,55] The following few sections investigate studies in the different regimes in more depth.

1.6.2 Solid / Electrical Solubility

Over the years there have been many studies that have concentrated on the diffusion of arsenic. In these studies, there have been many debates as to whether or not arsenic exhibits transient enhanced diffusion. Some authors present evidence that the diffusion difference is within the error of the measurement techniques used, some claim that there is TED, while others claim the TED seen in arsenic has been confused with the standard concentration dependent diffusion effect.[56]

Hoyt *et al.*[57] found that they could model their own experimental data along with data from the literature with an effective diffusivity that included arsenic diffusing with a neutral, a single negatively charged vacancy, and a doubly charged vacancy. They found that for concentrations below $2x10^{20}$ cm^{-3} that they only needed to include the neutral and the singly charged vacancy components in the effective diffusivity equation or that

$$D_{eff} = D_0 + D^{-}\left(\frac{n}{n_i}\right) \tag{1.17}$$

in order to fit the data well. When the arsenic concentration was increased to greater than $2x10^{20}$ cm^{-3} then the addition of a second term was needed so that

$$D_{eff} = D_0 + D^{-}\left(\frac{n}{n_i}\right) + D^{=}\left(\frac{n}{n_i}\right)^2 \tag{1.18}.$$

All of the profiles fit were for rapid thermal annealing data at temperatures greater than 1000°C.

Another primary focus of research has been on the activation and deactivation processes. Studies of other dopants have shown that the dopant can become fully active up to the solid solubility limit where precipitation begins and deactivation follows. Arsenic has been shown to

start the deactivation process well before the solid solubility limit is reached.[58]

Nobili *et al.*[58] performed experiments that compared the electrical deactivation of arsenic with the formation of arsenic precipitates. Silicon samples were implanted with 100 keV arsenic at doses ranging from $5x10^{15}$ up to $1x10^{17}$ cm^{-2}. The samples were next laser annealed at energies sufficient to melt the implanted region. By melting the implanted region, the arsenic atoms are able to go into solution, which allowed for complete activation of the dopant atoms. TEM shows no crystalline defects after laser annealing. The fully activated samples were then annealed in temperature regimes where the solid solubility is exceeded and precipitation occurs. Using electrical measurements it was determined that only a two-phase equilibrium, that is the formation of precipitates, is compatible with the results. Results from channeling studies showed that the precipitates had to be coherent with the silicon matrix. Because the precipitates had to be coherent, little to no strain field is associated with the precipitates and therefore TEM techniques for viewing are hindered. Small angle x-ray scattering (SAXS) was used to verify the existence of the precipitates and moreover that they were in the shape of thin platelets.

Using samples processed in a similar manner to Nobili *et al.*[58], Armigliato *et al.*[59] were able to view some form of precipitate using TEM. TEM observations of samples annealed at 450°C for 4 hrs showed that small defects were visible upon annealing. The small defects were depicted as precipitates on the basis of the large amount of arsenic that was deactivated. In addition, the defects were determined to be in the shape of platelets, which was in agreement with the findings of Nobili *et al.*[58] {311} defects were also visible, however no dislocation loops formed at this condition. Samples annealed at 900°C for 30 min showed precipitates in platelet form as well as dislocations and loops. Further investigation showed that assuming an SiAs composition for the precipitate could not fully explain the amount of deactivation seen in the electrical measurements. The remaining arsenic content was said to lie in particles that were of a smaller size than could be imaged by the TEM.

Wu *et al.*[60] looked into the formation of dislocation loops in more detail. Using 100 keV, $5x10^{15}$ cm^{-2} arsenic implants followed by anneals at 600°C, they showed that two distinct layers of loops form. A layer of loops formed at the projected range of the implant and another formed at the end or range. The results showed that the projected range loops formed due to exceeding the solubility limit. The projected range loops grew rapidly in size and were said to glide to the surface. The presence

of oxygen was also shown to have a large effect on the pinning of the loops.

Jones *et al.*[61] did a study similar to that of Wu *et al.*[60] and found similar results. They showed that the dissolution of arsenic precipitates lead to the growth of half loops. It was shown that arsenic doses above the solubility limit produced loops and half loops at the projected range upon annealing. Further annealing caused the loops to dissolve and the half loops to grow. In difference to Wu *et al.* it was suggested that the loops were not gliding to the surface, rather they were just dissolving via climb. It was also shown that the number of atoms bound by the projected range loops was insufficient to account for the entire growth of the half loops. Continued analysis lead to the result that dissolution of arsenic clusters could provide a sufficient number of interstitials to account for the half loop growth.

Hsu *et al.*[54] also saw a two-layered structure after an arsenic implant and anneal. They concluded that the dissolution of loops at the projected range for high dose implants was due to the injection of vacancies from the precipitates. To this day it is still unsettled as to the exact nature of the dissolution of the loops at the projected range. No experiments have been performed to solely determine if the dissolution is due to injection of vacancies from the arsenic precipitates or are the

precipitates a strong sink for interstitials that are supplied by the dissolution of the loops.

Nobili *et al.*[62] has suggested that arsenic displays both an electrical and solid solubility limit, with electrical inactive clusters being responsible for the difference. The electrical solubility limit has been shown to be dependent on the equilibrium carrier densities and have an exponential dependence on the annealing temperature given by:

$$n_{e(As)} = 2.2x10^{22} \exp\left(\frac{-0.47}{kT}\right) \tag{1.19}$$

where kT is in eV.

To further understand arsenic deactivation Rousseau *et al.*[49-51,63-65] investigated arsenic concentrations around the electrical solubility limit but below the precipitation limit, to determine the deactivation reaction. They showed that with laser annealing very high activation levels could be achieved. However, when subsequent annealing was performed around 750°C, a significant amount of deactivation was observed. This is an important finding because in the processing steps that go into building a device, the wafer may see many annealing steps of a similar temperature, which can lead to device degradation. Rousseau postulated that the deactivation process was due to the formation of a vacancy cluster via an

interstitial kick-out mechanism first described by Fair *et al.*[66,67] Fair *et al.*[66,67] described the kick-out mechanism as

$$As_nSi \Leftrightarrow As_nV + I \tag{1.20}$$

where As_nSi represents n (integer 1-4) arsenic atoms around a silicon lattice site, As_nV represents a deactivated cluster with a vacancy, and I represents an interstitial. A vacancy complex was further confirmed by Subrahmanyan *et al.*[68] They showed the importance of vacancies in the deactivation process by injecting either interstitials or vacancies from the surface and noting a retarded or enhanced deactivation rate, respectively. *Ab initio* calculations confirm the As_4V cluster to be energetically favorable compared to isolated arsenic atoms in the lattice.[69]

Rousseau *et al.*[50] went on to compare the deactivation that was observed with the enhanced motion of a boron spike. If Equation 2.4 was responsible for deactivation, then there should be a relationship between the deactivation and an enhanced motion of a boron spike due to the injection of an interstitial from the clustering reaction. It was shown that the time transients of the enhanced diffusion of the boron spike correlated with the deactivation process therefore supporting the proposed reaction.

Alternative clusters to the As_4V were suggested through modeling by Berding *et al.*[47] They reported that entropy considerations disfavor the formation of such a large complex and proceeded to do a complete free energy calculation to determine the role of As_4V in the deactivation process. Their findings showed that VAs_3Si_i and VAs_2Si_2 clusters could be equally as effective at deactivation as was the neutral As_4V. They concluded that because As_4V clusters are not needed to account for deactivation, materials with similar arsenic concentrations and deactivation fractions can have different microscopic states and therefore behave differently in subsequent processing steps.

Dokumaci *et al.*[52] made TEM observations that further support the findings of Rousseau.[49-51,63-65] Dokumaci *et al.*[52,70,71] showed that a reduced enhancement for larger concentrations of arsenic was due to the formation of dislocation loops. It was stated that even though a greater amount of interstitials were "kicked-out" at the higher arsenic concentrations, the loops acted as barriers to interstitial motion and therefore less enhancement was observed. It was also shown that there was a strong dependence of the density of dislocation loops on the amount of deactivation observed. Although the number of atoms bound by the defects was insufficient to account for all the inactive arsenic at all arsenic doses, the data still supports the idea that the loops are formed

due to the interstitials kicked-out during the deactivation process. Since the loop layer could not contain all the interstitials released from the clustering reaction, the remaining interstitials were available to enhance the diffusion of the boron marker layer.

1.6.3 Below Electrical Solubility

Few experiments have been done at arsenic concentrations below the electrical solubility limit because the effects of transient enhanced diffusion and dopant activation are less problematic. However, to build physical models for implantation damage, it is necessary to separate the effects of high-concentration diffusion, extended defects, and point defects. Therefore it is important to understand how the silicon interstitials interact with dopants and how this affects TED and activation. Park *et al.*[72] did a low dose experiment in which no TED of arsenic was detected. It was concluded that either the enhanced diffusion was below detectable limits or that the motion of arsenic is due to vacancies. In their study, the movement of the dopant profiles was the only consideration and no correlation to extended defects was mentioned.

In a separate experiment performed by Haynes *et al.*[37], boron doped wells of varying concentration with a single silicon implant were

used to examine how boron behaves in a supersaturation of silicon interstitials. Haynes *et al.*[37] used the experiments as a novel way to show that a B_sB_i pair can compete directly with {311} defects to retain available interstitials. After an anneal, the number of interstitials trapped in {311} defects was recorded as a function of well concentration ($[I_{311}]_B$). For the same anneal time and temperature, it was shown that as the boron concentration increases the number of interstitials trapped in {311} defects decreased. A silicon control sample with no boron was used to obtain the initial number of interstitials trapped in {311} defects ($[I_{311}]_0$) for the silicon implant condition used.

A simple model was used where the combination of a mobile B_sSi_i pair plus a Bs leads to a B_sB_i pair and releases the silicon interstitial ($B_sSi + B_s \Leftrightarrow B_sB_i + Si$). According to this reaction, the missing interstitial dose, $[I_{311}]_0$-$[I_{311}]_B$, is equal to $[B_sB_i]$ and proportional to $[B]^2$. Using this model a best-fit quadratic dependence on [B] was obtained. It was concluded that one interstitial is stabilized by the formation of an interstitial-substitutional B_sB_i pair.

This experiment provided a simple model for explaining the loss of interstitials with an increase in background boron concentration. Although a small cluster was used in the model, higher-order clusters are not ruled out and an upper bound for the boron cluster size was

determined. The results of this experiment are in accordance with other experiments that have shown that the BsBi cluster can exist. The BsBi configuration has been observed by deep-level transient spectroscopy[73] and *ab initio* calculations have indicated that the cluster is both bound and immobile,[74] as was assumed by the authors.

1.7 Thesis Statement

This work has contributed information in the following areas:

1. The study of {311} defect formation in the presence of an arsenic background.
2. Quantitative TEM studies of the annealing kinetics of {311} defects in an arsenic background.
3. Experimental investigation of the interaction between arsenic atoms and silicon interstitials.
4. Experimental investigation into the dissolution of arsenic-interstitial clusters.
5. Experimental investigation into the injection of vacancies from arsenic doped region.
6. Modeling of {311} formation and dissolution in the presence of an arsenic background.

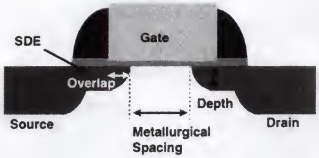

Figure 1.1. Typical CMOS transistor and terminology that describes the device.[75]

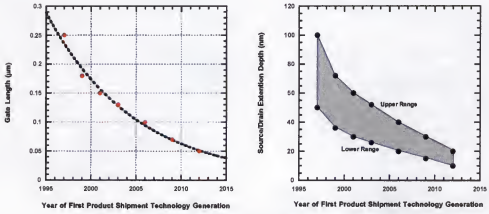

Figure 1.2. Semiconductor Industry Association (SIA) roadmap for transistor gate length and source/drain extension junction depth.[1]

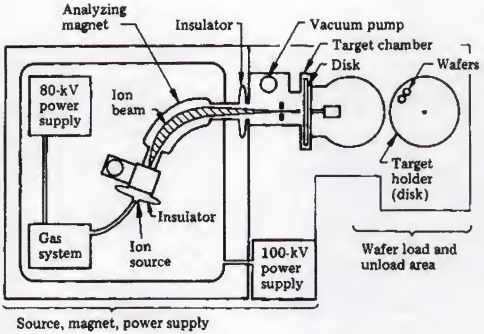

Figure 1.3. Typical commercial ion-implantation machine.[22]

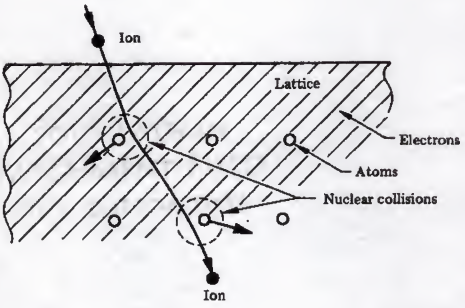

Figure 1.4. An incident ion can loses energy by nuclear collisions and collisions with electrons.[22]

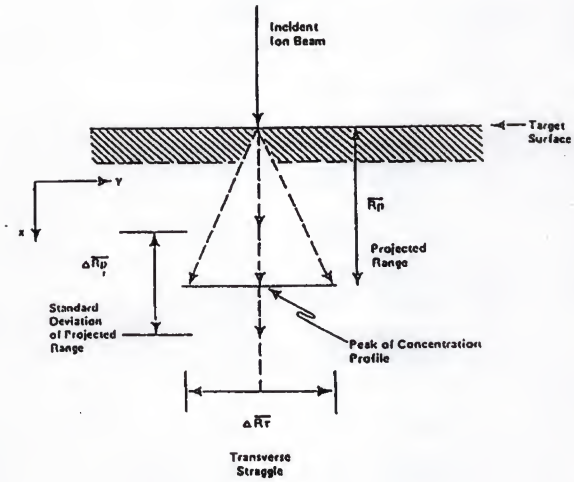

Figure 1.5. Critical ion implantation parameters

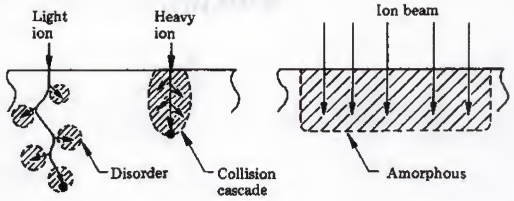

Figure 1.6. Disorder produced from light and heavy ions and the formation of an amorphous region.[22]

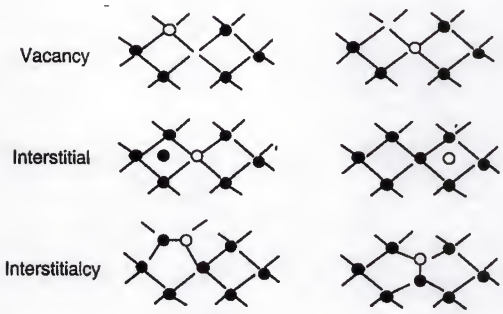

Figure 1.7. Possible dopant diffusion mechanisms

CHAPTER 2
EFFECT OF ARSENIC ON {311} FORMATION AND DISSOLUTION

2.1 Introduction

As devices continue to be scaled to smaller and smaller dimensions, the dopant diffusion begins to control the depth of the electrical junction. As discussed previously, Transient Enhanced Diffusion (TED) adversely affects the diffusion of dopants and becomes an important parameter to consider in the process design of future devices. TED from self-implants has been a heavily studied area for many groups and a correlation has been made between TED and extended defect formation and dissolution. Eaglesham *et al.*[39] has suggested that extended defects serve as storage sites for excess interstitials and that during the dissolution of the defects interstitials are released. Once released, the interstitials are free to interact with any dopant atoms present. Common dopant atoms are known to fully or partially diffuse via interstitials and therefore the release of interstitials propels the enhanced diffusion of the dopant atoms.

The addition of excess interstitials to regions doped with either boron or phosphorus has been shown to have a measurable influence on the nucleation, growth and dissolution of extended defects. To

understand the influence the dopant has on the defect processes, studies were brought about to examine the interstitial trapping by impurity dopants. Haynes *et al.*[37] executed a study of boron interstitial trapping using boron-doped wells. In their experiment they formed various concentration, boron well structures and added excess interstitials by way of silicon self-implants. Subsequent anneals were done to nucleate, grow and eventually dissolve {311} defects. It was determined that for boron concentrations above $1x10^{18}$ cm^{-3} the boron traps the interstitials and causes a reduction in the {311} formation. It was also found that once the defects formed the boron concentration did not affect the dissolution process. Similar results were found for phosphorus by Keys *et al.*[43]

Unlike boron and phosphorus, which are known to be pure interstitial diffusers, arsenic is known to diffuse by both interstitial and vacancy mechanisms. Only being a partial interstitial diffuser, arsenic was likely to have a lesser effect on the {311} defect processes. However, even with being a partial diffuser, there should still be sufficient reduction in the nucleated {311}'s. To gain knowledge on how arsenic effects the {311} nucleation, growth and dissolution process, similar experiments to those of Haynes *et al.*[37] and Keys *et al.*[43] were devised. To cover the a range of concentrations below the clustering limit, doped arsenic wells ranging in concentrations between $1x10^{17}$ and $1x10^{20}$ cm^{-3} were created

and excess interstitials were added using a silicon self-implant known to cause {311} defects in undoped silicon. To study the effects of the arsenic, the formation and dissolution of {311} defects that formed upon low temperature annealing, was monitored as a function of arsenic concentration. The ensuing sections will report the results from such an experiment and discussions of the implications of the data are presented.

2.2 Experimental Overview

2.2.1 Arsenic Well Formation

Arsenic wells were fabricated using the following process. Presented in Figure 2.1 is the schematic view of the process that follows. Six p-type epi-silicon wafers were pre-amorphized with silicon such that the damage from following arsenic implants will be equalized and channeling reduced. A double implant was used for the pre-amorphiztion step to ensure a deep amorphous region. The preamorphization implant was done on a Varian E1000 with a beam current of around 4 mA. The temperature of the wafer was held to about 90°C. A deep pre-amorphization was formed using silicon implanted at an energy of 200 keV and dose of $2x10^{15}$ cm^{-2}. A subsequent shallow pre-amorphiztion was done using a silicon implant at an energy of 70 keV and a dose of $1x10^{15}$ cm^{-2}. Following the pre-amorphization step, Arsenic was

implanted into the amorphized region. Implant energies of arsenic were chossen such that the implant profiles would be fully contained within the amorphous region before annealing. Also, a double implant was used at each well condition such that after annealing a constant concentration of arsenic would be established. Deep arsenic implants were incorporated at an energy of 200 keV and at doses of $1.6x10^{12}$, $4.8x10^{12}$, $1.6x10^{13}$, $4.8x10^{13}$, $1.6x10^{14}$, $4.8x10^{14}$ cm^{-2}. Following the deep implants, shallow arsenic was implanted at an enrgy of 70 keV and at doses of $8.5x10^{11}$, $2.5x10^{12}$, $8.5x10^{12}$, $2.5x10^{13}$, $8.5x10^{13}$ and $2.5x10^{14}$ cm^{-2}, respectively. The lowest dose samples showed identical results to that of a silicon control, thus the $3x10^{17}cm^{-3}$ ($4.8x10^{12}$ cm^{-2} + $2.5x10^{12}$ cm^{-2}) sample was used as the control from this point forward. All six wafers were then annealed in a furnace under nitrogen ambient at 550°C for 60 min to regrow the amorphized layer. A subsequent 60 min furnace anneal at 1100°C in nitrogen ambient was performed to form a constant arsenic concentration to a depth in excess of 1600Å. The total arsenic implant doses used were $2.5x10^{12}$, $7.3x10^{12}$, $2.5x10^{13}$, $7.3x10^{13}$, $2.5x10^{14}$ and $7.3x10^{14}$ cm^{-2}, which formed wells with concentrations of $2.0x10^{17}$, $4.0x10^{17}$, $1.1x10^{18}$, $3.5x10^{18}$, $1.1x10^{19}$ and $3.0x10^{19}$ cm^{-3}, respectively.

Figure 2.2 shows the results from the Secondary Ion Mass Spectroscopy (SIMS) analysis, following the 1100°C well anneal. The SIMS

was done using a 5.5keV cesium beam and a sputter rate of 5.8±0.5 Å/sec (200 nA). The raster area was set at 500 μm x 500 μm and the crater depths were measured using a stylus profilometer. The atomic concentrations of arsenic were calculated from relative sensitivity factors determined from standard samples.

Following the well anneals the wafers were sectioned using a diamond scribe and oxide etched to remove any oxide formation that occurred during the annealing cycles. The oxide etch used was a 6:1 HF buffered oxide etch. Following the oxide etch the samples were sent to Kroko Ion Implantation Services for silicon ion implantation. There each sample was independently implanted with silicon at an energy of 40 keV and dose of $1x10^{14}$ cm^{-2}. These conditions were used because they are known to cause {311} defect formation after subsequent annealing.

After silicon implantation each sample was further cored into 3mm diameter discs, to be used as Transmission Electron Microscopy (TEM) specimens, using a Gatan ultra-sonic disc cutter. Each sample was then furnace annealed under nitrogen ambient at various temperatures and times as listed in Table 2.1.

After furnace annealing plan-view TEM specimens (PTEM) were prepared by an HF etch process. This process consists of backside grinding until the sample is approximately 100 μm thick using aluminum

oxide powder and water. After grinding, the surface is protected using a low melting temperature wax. After covering the surface with wax the backside of the sample is exposed to a HF etchant (3:1 HNO_3:HF) via a drip etch system. The etchant is applied until a small hole and suitable thin area is seen under white light. With practice and patience, the thin area surrounding the hole will be electron-transparent. Once the etching process is completed, the wax is removed by immersing the sample in Heptane (C_7H_{16}) for 20 or more minutes. The samples were subsequently air-dried and are then ready for viewing in the TEM.

After PTEM sample preparation the samples were analyzed using a JEOL 200CX TEM. In order to increase the contrast of the defects in relation to the background, all samples were imaged using a weak beam dark field (WBDF) mode. In most cases the g220 reflection was used to acquire the necessary images. A magnification of 50,000X was used for all plan view analysis. Since only limited cross section samples were used in this study, the procedure will not be discussed within. However, presented in Figure 2.3 is a cross-section TEM image that shows the {311} defects at a depth centered at ~700Å and the amorphous/crystalline interface for the arsenic well at ~3900Å.

2.2.2 End of Range Loops from Preamorphization

End of range (EOR) dislocation loops from the preamorphization of the silicon substrate remained after the 1100°C 60 minute anneal at a depth of ~4000Å. The size and distribution of the EOR defects was constant for all the specimens. There was no difference in the {311} formation or dissolution for the control sample with no preamorphization and the control with the EOR loops from preamorphization. This implies the EOR defects were sufficiently removed from the self implanted region and thus had no effect on the {311} formation or dissolution process, which is consistent with previous experiments.[76] Figure 2.3 is a TEM micrograph that shows a cross sectional view of the process area. The {311} defects of study are at ~700Å below the surface and the EOR loops are much deeper around 4000Å.

Table 2.1. Experimental Matrix for arsenic well study

Concentration (cm^{-3})	700°C	750°C	800°C
$1x10^{17}$		15, 30, 45, 90 min	
$3x10^{17}$	45, 275, 720 min	15, 30, 45, 90 min	5, 10, 15 min
$1x10^{18}$		15, 30, 45, 90 min	
$3x10^{18}$	45, 275, 720 min	15, 30, 45, 90 min	5, 10, 15 min
$1x10^{19}$		15, 30, 45, 90 min	
$3x10^{19}$	45, 275, 720 min	15, 30, 45, 90 min	5, 10, 15 min

2.3 Defect Analysis

2.3.1 Image Analysis

There are many methods to analyze the TEM images of the different defect states. Three of the more useful methods are to investigate the change in length, the distribution of defect sizes and the total number of defects. The change in total length leads to the knowledge of how many interstitials make up a series of defects. The distribution of defect sizes relays important information about the coarsening process of the defects. The total number of defects gives a value of how many defects are in an anneal step.

For quantitative analysis of defect sizes and densities, the TEM micrographs taken at 50,000X were enlarged by a factor of three to a magnification of 150,000X. The defects were then traced on transparency and scanned into a computer for image processing. Adobe Photoshop and NIH image were used to scan and count the defects. This data was further processed to determine the number of defects and the approximate number of interstitials trapped by the defects. The process is described in more detail in a previous publication by Bharatan *et al.*[77] This data was then plotted versus various experimental parameters that are discussed in the remaining sections in this chapter.

2.3.2 Effect of Arsenic on Trapped Interstitial Values

Plan-view TEM images are presented in Figures 2.4-2.13 of {311} defects that remained in arsenic concentrations of $3x10^{17}$, $3x10^{18}$ and $1x10^{19}$ cm^{-3} after each annealing step listed in Table 2.1. In each of the micrographs, the bright rod-shaped segments represent the {311} defects. Each of the defects is made up of a number of interstitials. Prior studies have shown that if the defects are on average 40Å wide then their structure leads to 26 silicon interstitials per nm of length under the specified annealing conditions [39]. The defects in this study average about 40Å and therefore the 26 interstitials per nm was used in all defect calculations.

In all of the images in Figures 2.4-2.13 the length of each defect was measured and by addition of each measurement the total length of defects was determined. Knowing that there are 26 interstitials per nm of length in the {311} defects, the length calculation can be converted to the total number of trapped interstitials in each sample. Figures 2.14-2.16 present the results at each temperature and annealing time, as plots of the number of trapped interstitials versus arsenic concentration.

In these figures it is apparent that there is a significant effect on the number of interstitials trapped in {311} defects at higher arsenic concentrations. As the concentration of arsenic is raised the number of

interstitials in {311} defects is decreasing. As with the other dopants studied in a similar manner, it appears that arsenic is pairing with interstitials and acting as an alternative site. Eaglesham *et al.*[39] has stated that the release of interstitials from the defects over time has a direct correlation to TED. From this study it is now known that the defect nucleation is affected by the presence of arsenic. The effect this has on TED will be seen in how the defects that remain act upon dissolution.

2.3.3 Effect of Arsenic on {311} Defect Dissolution

The {311} dissolution process happens by the release of interstitials from the defects. The net loss of interstitials from the defects occurs as an exponential decay with time and can be expressed as

$$Si_i(t) = Si_0(0)\exp\left(-K_{311} * t\right) \qquad (2.1).$$

In equation 2.1 $Si_i(t)$ is the trapped interstitial concentration per area as a function of time, $Si_0(0)$ is the concentration per area at time zero, K_{311} is the {311} dissolution rate constant and t is time. By carrying out several measurements at various temperatures and arsenic concentrations a family of decay curves may be generated. Determination of the parameters in Equation 2.1 can be accomplished by plotting the {311}

trapped interstitial counts versus annealing time and then fitting each series of data points with an exponential curve. The two most important values are the slope, which represents the K_{311} value and the Y-intercept that denotes the initial number of interstitials.

In Figures 2.14-2.16 it was shown that increasing the arsenic concentration leads to a decreased number of interstitials in defects. From the figures it is also seen that with increasing annealing time, the number of interstitials in the defects is decreasing which shows the defects are in a state of dissolution. To look at how the arsenic affects the dissolution, the number of trapped interstitials was plotted as a function of annealing time at each concentration. These plots are presented for 700°C, 750°C and 800°C in Figures 2.17, 2.18 and 2.19, respectively.

The data points were fitted with exponential least-squares fits and the dissolution rate constants were extracted. The dissolution time constant for this experimental was calculated to be 50±5 min for each concentration. The time constant obtained in this experiment is consistent with the time constants of {311} studies previously reported.[30,36,39,43,44,78]

Having a similar dissolution time constant at all temperatures supports the idea that the {311} dissolution is not effected by the

presence of arsenic. It may also be recognized that at each arsenic concentration the Y-intercept value is independent of annealing temperature. However, when each concentration is compared there is a large reduction in the Y-intercept value for increased arsenic concentrations. This effect will be discussed in the following section.

2.3.4 Effect of Arsenic on the "Plus One Model"

In studies on {311} defect dissolution the initial number of interstitials was independent of anneal conditions, suggesting it was a function of the implant conditions. Previous studies on {311} defects have shown that the Y-intercept or $Si_0(0)$ has related closely to the plus one model. The plus one model assumes that after Frenkel pair recombination there will be a dose of interstitials that remains that is equal to the implanted dose. The plus one model appears to be independent of dose or anneal conditions.

The implanted dose in this experiment was $1x10^{14}$ cm^{-2} and in the control samples the $Si_0(0)$ value hovers around $7X10^{13}$ cm^{-2}, which is in close agreement to the model. As the arsenic concentration was increased, a reduction in the Si_0 (0) value resulted. The realization of this data is that some sort of arsenic-interstitial complex is created during the initial stages of annealing. With less interstitials available at nucleation due to a dopant-interstitial complex formation, a decrease in the number

of trapped interstitials in {311} defects is eminent. The structure and binding energy of the complex has not been disclosed at this time. Modeling efforts presented in Chapter 4 help to decipher some of this information. However, there are a couple schools of thought on the strength of the bond between silicon interstitials and an arsenic atom. First, it could be that the complex is more stable than the {311} defects. In this case the complexes would hold interstitials until an energy sufficient was present and the interstitials would be released. This would most likely happen after the dissolution if the {311} defects and so the release from the pairs would not affect the dissolution. It is also possible that the defect complex is less stable and that the dissolution of the {311} defects is dependent only on the defect itself. In other words, the release of interstitials from {311} defects by how fast the interstitials that make up the defect are able to diffuse away. In this view, the dissolution of the {311} defect is based on how fast the interstitials can leave the ends of the defects and the release of interstitials from the As-I complexes would not affect the dissolution rate either. Another view may be that the {311} defects have a supersaturation of interstitials surrounding them. When interstitials diffuse away then the defects release the interstitials to satisfy the supersaturation requirements. In this instance the release of interstitials from As-I complexes would affect

the dissolution. Assuming that there are enough interstitials in the complexes to cause an effect, the release of the interstitials from the complexes would supply the {311} with the need interstitials to keep the supersaturation satisfied. If there were more interstitials released from the complex formations than from {311} defects then a delay in dissolution would occur. This is not seen experimentally and therefore is not believed to be true. A final scenario may be that with the addition of arsenic the Fermi level is raised to a point where the interstitials diffuse out of the area before they are captured by the {311} defect. This is not believed to be true since this same experiment was done with a number of different dopants and different results were acquired in each case. The true answer can not be obtained from this experiment alone. Additional experiments presented in the next few chapters are presented in hopes of obtaining the answers.

2.3.5 Activation Energy Calculations

The activation energy for the dissolution of {311} defects can be calculated using the dissolution kinetics experimental data. The activation energy is related to the dissolution rate constant by

$$K_{311} = K_{311}(0)\exp\left(\frac{-E_a}{kT}\right) \qquad (2.2).$$

In Equation 2.2, E_a is the activation energy, K is Boltzman's constant (8.616×10^{-5} eV/k) and T is temperature in Kelvin. Rearranging this equation gives the linear relation of

$$\ln(K_{311}) = \ln(K_{311}(0)) + \frac{E_a}{kT} \qquad (2.3).$$

So, by plotting K_{311} versus $1/T$ a straight line with a slope of E_a/k should result. Multiplying the slope by k results in the activation energy. The rate constants as a function of $1/T$ (K^{-1}) for each arsenic concentration are plotted in Figure 2.20. The activation energy for each concentration was calculated to be 3.4±0.2 eV. This activation energy is in the range of published values for {311} defects that range from 3.3 to 4.2 eV.[32,78,79] Again, there is no effect of arsenic on the dissolution kinetics of {311} defects. This seems to indicate that the dissolution of the defects is limited by either the release rate of interstitials from the ends of the defects or by the diffusion of interstitials away from the damage region. The addition of arsenic to the system has no effect on either of these mechanisms.

2.3.6 Effect of Arsenic on Defect Size and Density

Presented in Figures 2.21-2.23 is the effect arsenic has on the size distribution of {311} defects. For higher arsenic concentrations, not only do less defect form but they tend towards smaller sizes also. The smaller

sizes can be seen in a shift in the histograms to only include defects in the lower size ranges. Also, total defect density data as a function of annealing time at different arsenic concentrations is presented in Figures 2.24-2.26 for each annealing temperature. Apparent in these figures is the lack of change in overall defect density at each concentration. However, when the total number of interstitials trapped in the defects was calculated in the previous sections, the number of interstitials in the defects was decreasing with increasing arsenic concentration. The only way for these two to coincide would be to have smaller defects.

This may explain why the defects at higher concentrations are less stable. In most growth phenomena it is known that smaller defects grow at the expense of larger defects. A critical size is determined dependent on the energy of the system. If a defect is larger than the required size it will grow at the expense of the defects that are not of critical size. Once the smaller defects are dissolved the larger ones may then dissolve. This can be seen in the density plots at most of the concentrations. At small anneal times there is a number of small defects, as time evolves less small defects are realized and some larger defects are present. At some point the larger defects dissolve and at long times there are small and few defects.

2.3.7 Possible Arsenic Complexes

The data presented suggests that the introduction of arsenic is having a significant effect on the amount of excess interstitials available for {311} defects. There are several possible mechanisms that might account for this effect. Two of the more likely reasons include formation of arsenic clusters or enhanced diffusivity of charged interstitials when the material becomes extrinsic ($n>n_i$). First, as was suggested for boron, the arsenic could be trapping the excess interstitials in some form of a complex. A simple chemical equation that would relay the transfer of an arsenic atom and silicon interstitial into a dopant-defect complex may be developed as

$$As_x + Si_i \Leftrightarrow As_x I \tag{2.4}$$

In order to determine what the value of x may be the concept of missing interstitials is introduced. It is known that if there is no arsenic present the total number of interstitials available at time zero is on the order of $7x10^{13}$ cm^{-2}. As arsenic is added this number decreases. If it is assumed that all of the arsenic within the silicon implant damage region is interacting with the silicon interstitials then a missing dose of interstitials can be calculated. In this experiment the maximum depth of the {311} bottom of the defect layer was measured to be ~800Å by cross-sectional TEM. If this value is multiplied by the concentration of arsenic, the dose

of arsenic atoms affected by the excess interstitial dose is estimated. These values range from $2.4x10^{12}$ As/cm^2 for the $3x10^{17}$ cm^{-3} well to $2.4x10^{14}$ As/cm^2 for the $3x10^{19}$ cm^{-3} well. As previously stated, the dose of the interstitials injected by the silicon implant was determined to be ~$7x10^{13}$ cm^{-2}. The missing interstitial dose is then the difference between the y-intercept of the undoped well (~$7x10^{13}$ cm^{-2}) and the y-intercept of the doped samples in Figures 2.17-2.19. Since the percent change is the same at each temperature, only one temperature needs to be evaluated. A plot of the missing interstitial dose versus arsenic dose is presented in Figure 2.25. A few things are noticed when this graph is reviewed. First there is not a linear relationship throughout the concentration ranges. This is due to the fact that as the arsenic concentration is raised there becomes a point at which there are more arsenic atoms available than interstitials in the system. If the graph is broken into two sections then a number can be reached. The slope between the first two points turns out to be 0.5, which means that there is a 2:1 arsenic to interstitial ratio before a saturation of interstitial trapping is reached. Thus if arsenic trapping were occurring the cluster might be an As_2I. This is a crude estimate and other complexes with higher silicon to arsenic ratios might also be possible to explain the role

off in the curve. If the whole curve were assumed to be linear then an $As_{10}I$ would be the complex of choice.

2.4 Arsenic Effect on {311} Formation and Dissolution Summary

The effect of arsenic on {311} formation and dissolution was studied, by the formation of arsenic wells. Silicon implants known to cause {311} defects were introduced into the wells. After various anneals the formation and dissolution behavior of the defects was determined. It was determined that arsenic had a strong effect of the nucleation of the defects. With increasing arsenic concentration a decrease in the number of interstitials at zero time was captured. However, once formed the defects dissolved at the same rate independent of the arsenic concentration. The activation energy for dissolution also was not affected by the arsenic concentration. It was determined that in the initial stages of annealing As-I pairs were formed and provided alternate sites to {311}'s for the interstitials. These pairs break up in time but by the time they do the {311}'s are in a dissolution mode and since the {311} dissolution is mediated by the release rate at the ends of the defects, the breakup does not effect dissolution.

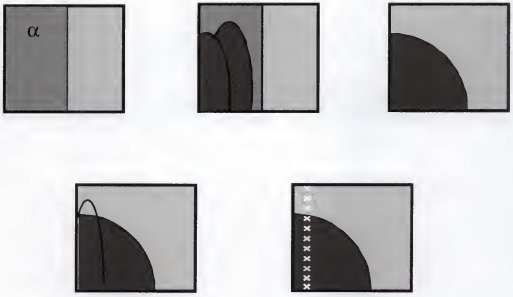

Figure 2.1. Process steps used in the design of an experiment to examine the effects of arsenic on extended defect nucleation and dissolution.

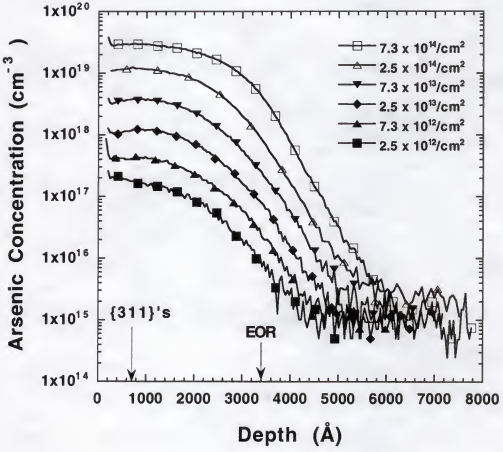

Figure 2.2. Secondary Ion Mass Spectroscopy (SIMS) plots of the arsenic wells after an 1100°C 60 min anneal.

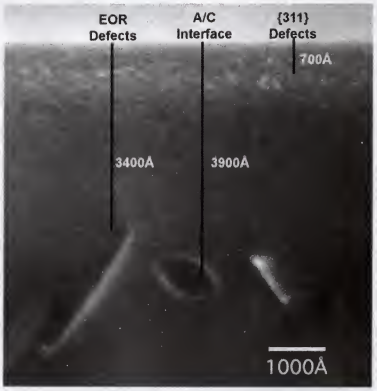

Figure 2.3. Cross-sectional TEM image of the processed region. A band of {311} defects is located ~700Å below the surface and large EOR defects are centered about 4000Å.

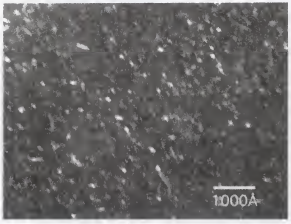

$3x10^{17}\,cm^{-3}\,As^{+}$

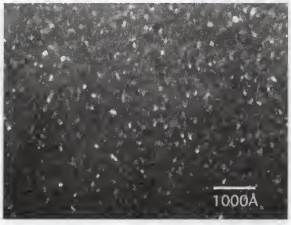

$3x10^{18}\,cm^{-3}\,As^{+}$

$3x10^{19}\,cm^{-3}\,As^{+}$

Figure 2.4. Effect of arsenic concentration on {311} defects formation: 700°C 45min

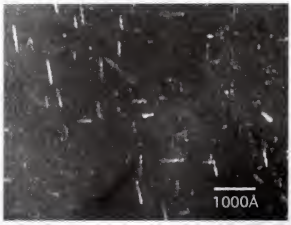

$3x10^{17}\,cm^{-3}\,As^{+}$

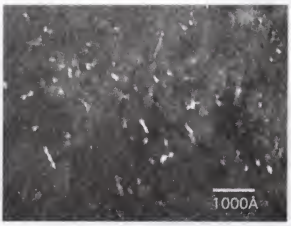

$3x10^{18}\,cm^{-3}\,As^{+}$

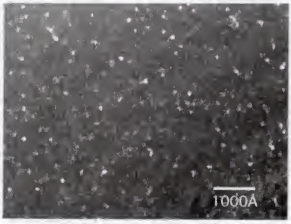

$3x10^{19}\,cm^{-3}\,As^{+}$

Figure 2.5. Effect of arsenic concentration on {311} defects formation: 700°C 275min

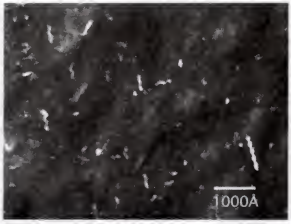

$3x10^{17}\ cm^{-3}\ As^{+}$

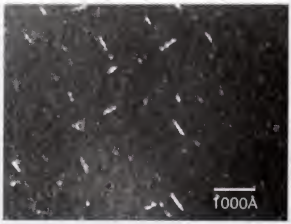

$3x10^{18}\ cm^{-3}\ As^{+}$

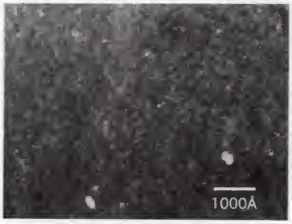

$3x10^{19}\ cm^{-3}\ As^{+}$

Figure 2.6. Effect of arsenic concentration on {311} defects formation: 700°C 720min

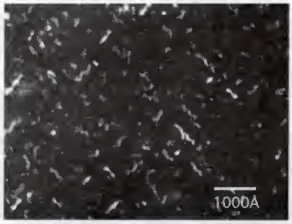

$3x10^{17}\,cm^{-3}\,As^{+}$

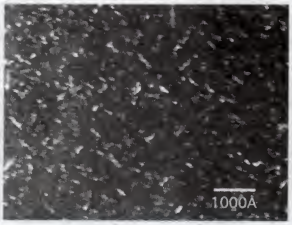

$3x10^{18}\,cm^{-3}\,As^{+}$

$3x10^{19}\,cm^{-3}\,As^{+}$

Figure 2.7. Effect of arsenic concentration on {311} defects formation: 750°C 15min

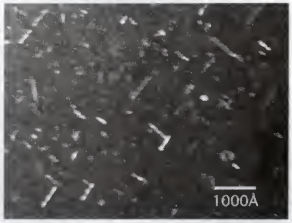

$3x10^{17}\,cm^{-3}\,As^{+}$

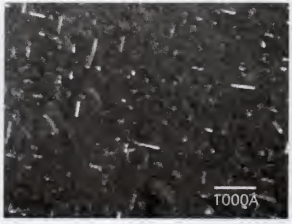

$3x10^{18}\,cm^{-3}\,As^{+}$

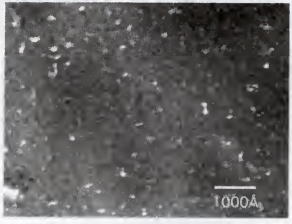

$3x10^{19}\,cm^{-3}\,As^{+}$

Figure 2.8. Effect of arsenic concentration on {311} defects formation: 750°C 33min

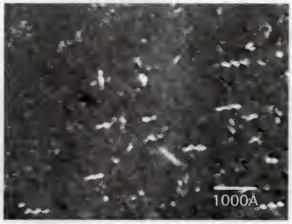

$3x10^{17}\,cm^{-3}\,As^{+}$

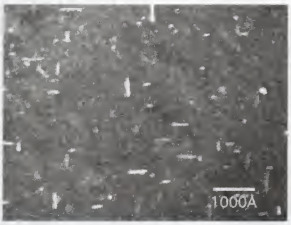

$3x10^{18}\,cm^{-3}\,As^{+}$

$3x10^{19}\,cm^{-3}\,As^{+}$

Figure 2.9. Effect of arsenic concentration on {311} defects formation: 750°C 45min

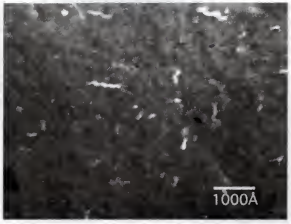

$3x10^{17}\,cm^{-3}\,As^{+}$

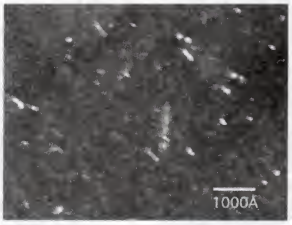

$3x10^{18}\,cm^{-3}\,As^{+}$

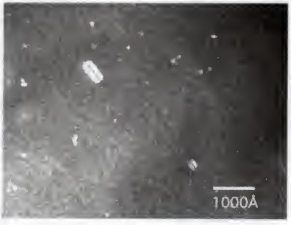

$3x10^{19}\,cm^{-3}\,As^{+}$

Figure 2.10. Effect of arsenic concentration on {311} defects formation: 750°C 90min

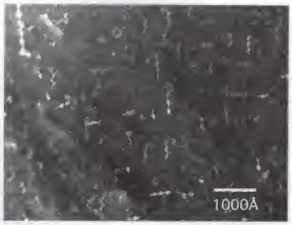

$3x10^{17}\,cm^{-3}\,As^{+}$

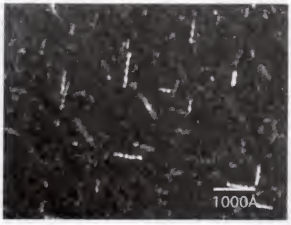

$3x10^{18}\,cm^{-3}\,As^{+}$

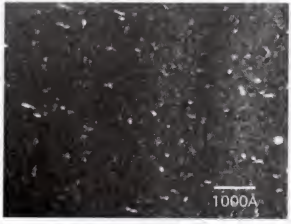

$3x10^{19}\,cm^{-3}\,As^{+}$

Figure 2.11. Effect of arsenic concentration on {311} defects formation: 800°C 5min

$3x10^{17}\,cm^{-3}\,As^{+}$

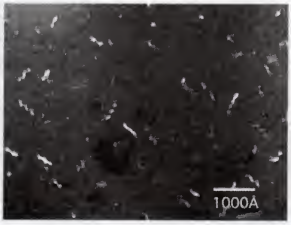

$3x10^{18}\,cm^{-3}\,As^{+}$

$3x10^{19}\,cm^{-3}\,As^{+}$

Figure 2.12. Effect of arsenic concentration on {311} defects formation: 800°C 10min

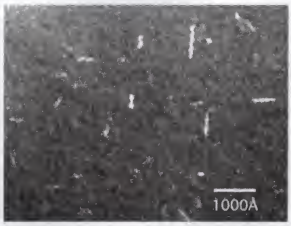

$3x10^{17}\,cm^{-3}\,As^{+}$

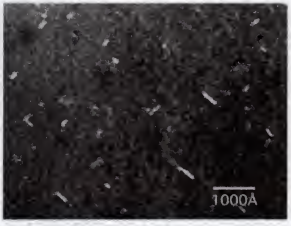

$3x10^{18}\,cm^{-3}\,As^{+}$

$3x10^{19}\,cm^{-3}\,As^{+}$

Figure 2.13. Effect of arsenic concentration on {311} defects formation: 800°C 15min

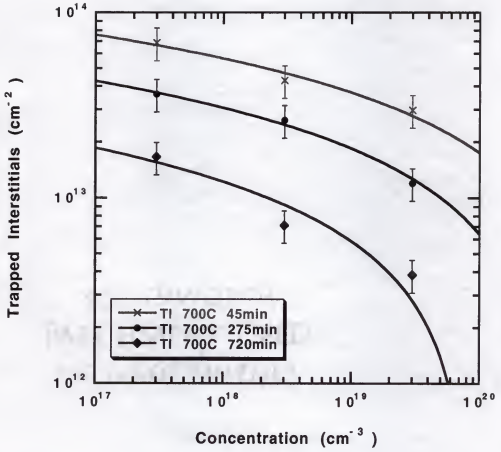

Figure 2.14. Number of trapped interstitials in {311} defects as a function of arsenic concentration after a 700°C anneal for various times.

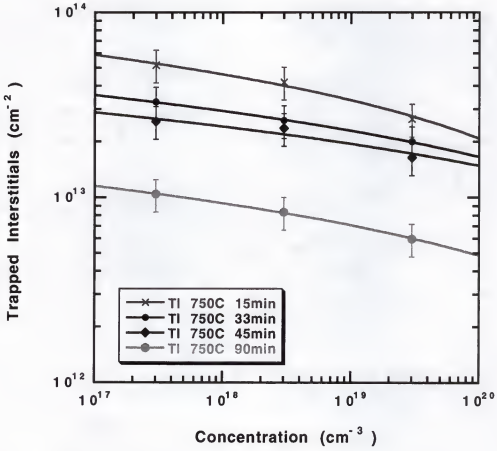

Figure 2.15. Number of trapped interstitials in {311} defects as a function of arsenic concentration after a 750°C anneal for various times.

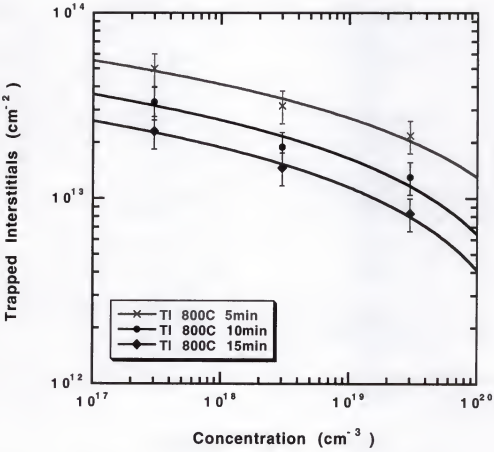

Figure 2.16. Number of trapped interstitials in {311} defects as a function of arsenic concentration after a 800°C anneal for various times.

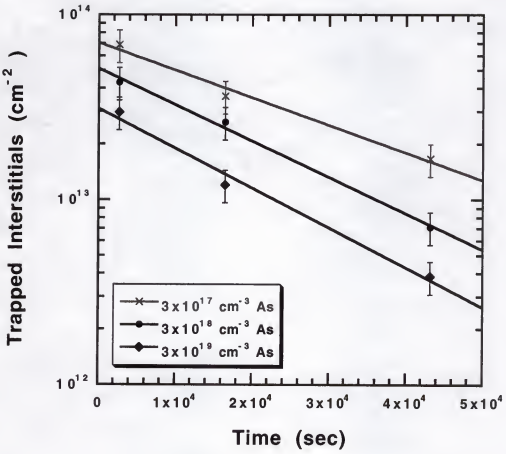

Figure 2.17. Effect of arsenic concentration on the {311} defect dissolution after furnace anneals at 700°C. A similar slope represents similar dissolution constants showing the arsenic has no effect on the dissolution.

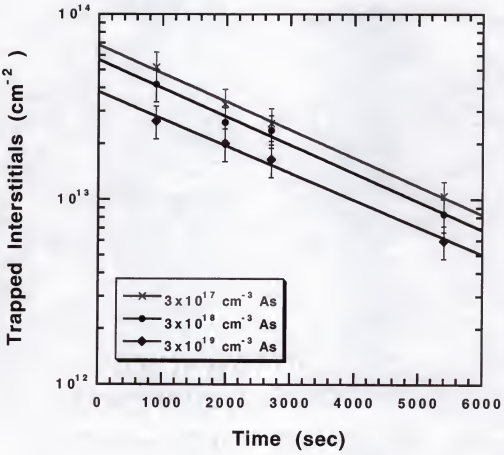

Figure 2.18. Effect of arsenic concentration on the {311} defect dissolution after furnace anneals at 750°C. A similar slope represents similar dissolution constants showing the arsenic has no effect on the dissolution.

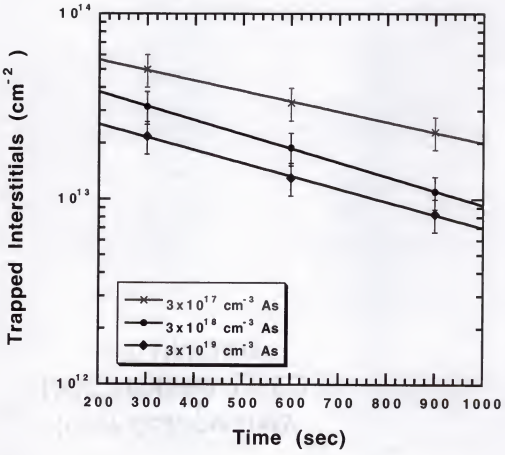

Figure 2.19. Effect of arsenic concentration on the {311} defect dissolution after furnace anneals at 800°C. A similar slope represents similar dissolution constants showing the arsenic has no effect on the dissolution.

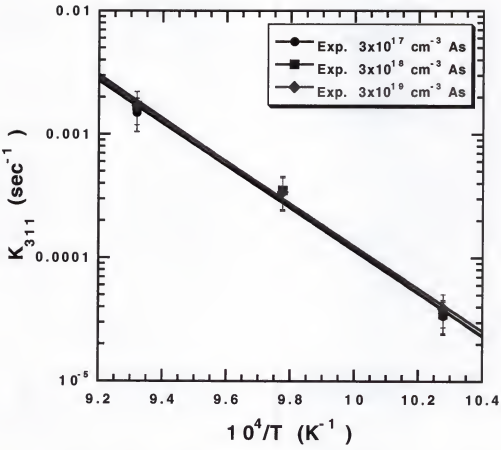

Figure 2.20. Plot of dissolution rate constants at various temperatures for activation energy calculations. The slope at each concentration is the same relaying that arsenic has no effect on the activation energy to {311} dissolution. The activation energy was calculated to be 3.4 ±0.2 eV, which is in the same range as previous studies on pure {311} dissolution.

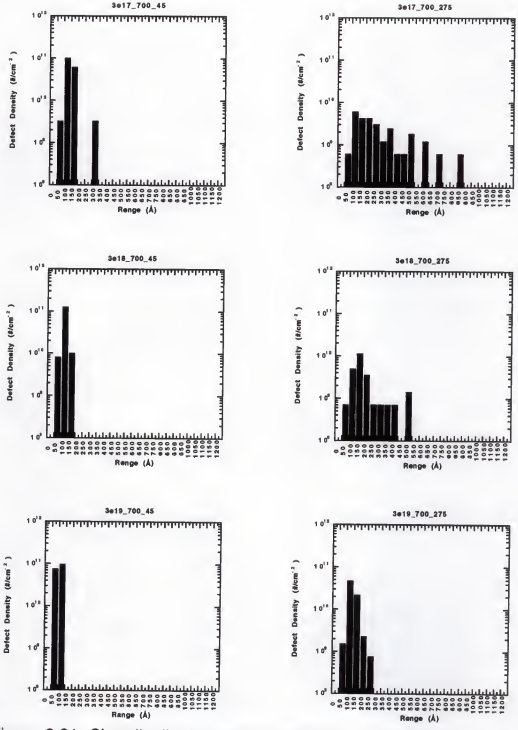

Figure 2.21. Size distribution data at various times at 700°C

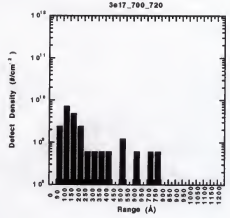

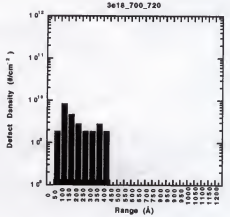

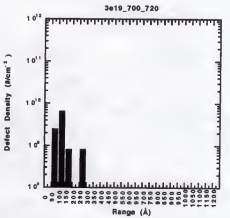

Figure 2.21. (Continued)

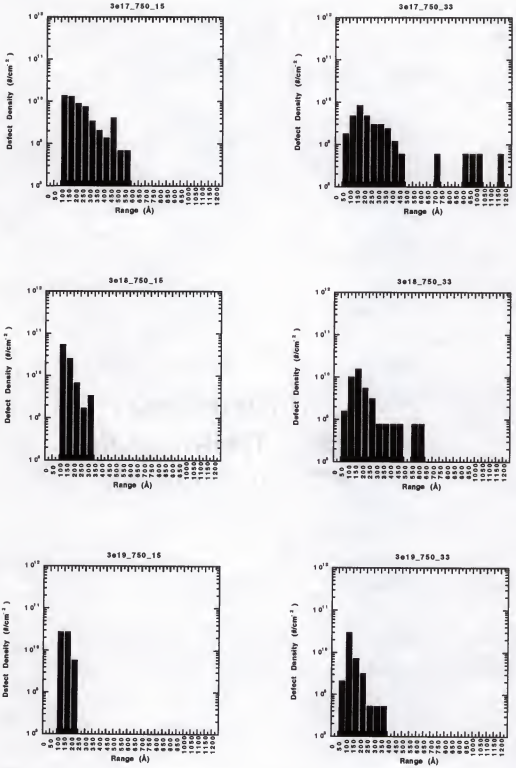

Figure 2.22. Size distribution data at various times at 750°C.

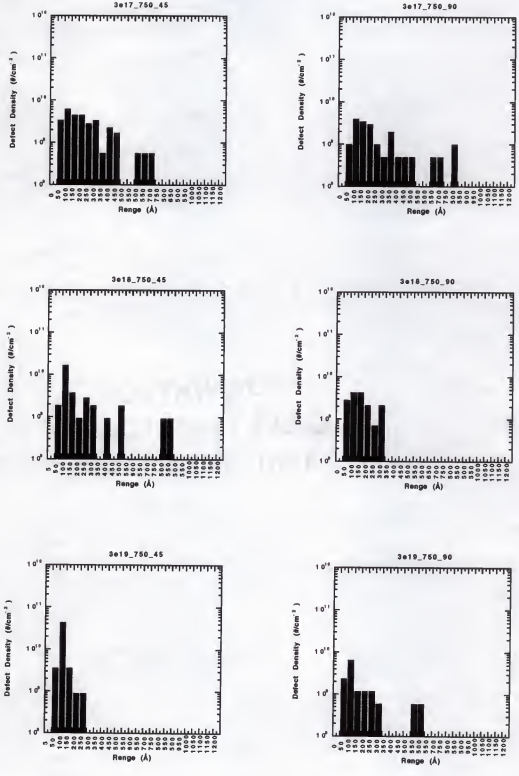

Figure 2.22. (Continued)

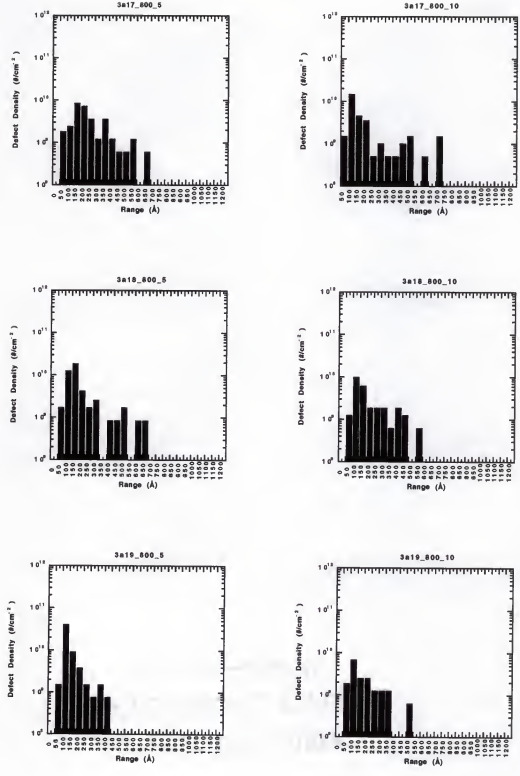

Figure 2.23. Size distribution data at various times at 800°C.

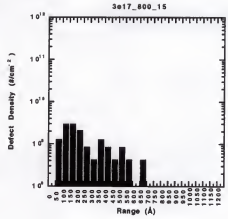

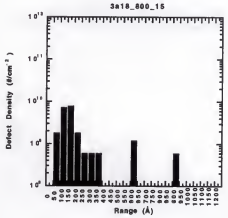

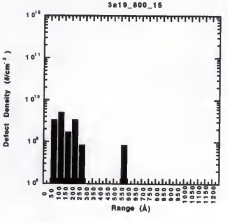

Figure 2.23 (Continued)

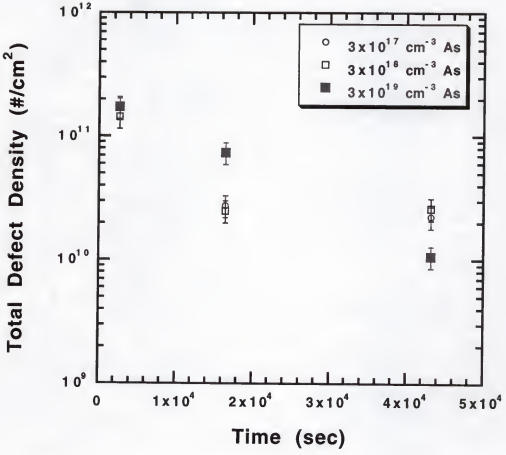

Figure 2.24. Total defect densities as a function of annealing times at 700°C for each arsenic concentration studied.

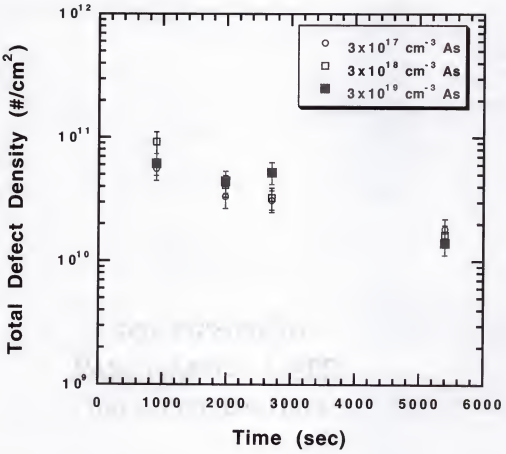

Figure 2.25. Total defect densities as a function of annealing times at 750°C for each arsenic concentration studied.

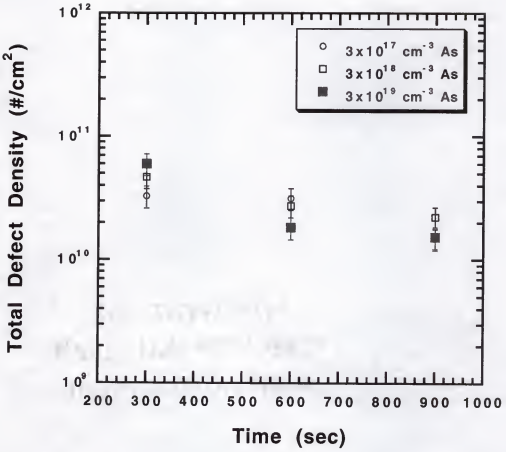

Figure 2.26. Total defect densities as a function of annealing times at 800°C for each arsenic concentration studied.

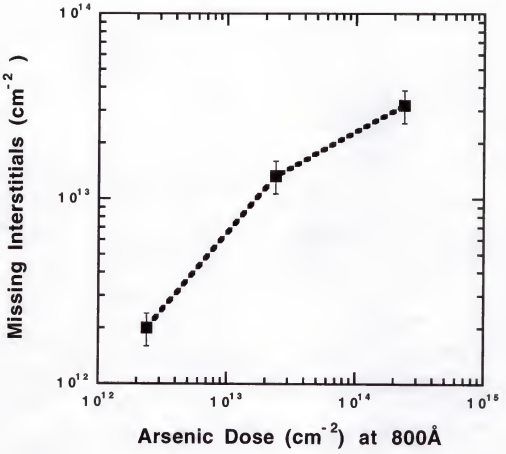

Figure 2.27. Missing interstitial dose as a function of the dose of arsenic available at 800Å. The slope of the initial portion of the curves is 0.5, which relates to a possible As_2I complex.

CHAPTER 3
RELEASE OF SILICON INTERSTITIALS AND VACANCIES FROM DOPED ARSENIC LAYERS

3.1 Boron Marker Layers

3.1.1 Overview

Gate length, gate dielectric thickness and junction depths are the primary parameters that control transistor performance. According to the Semiconductor Industry Association (SIA) roadmap junction depths and gate lengths will continue to decrease at a rapid rate in the years to come. With decreasing junction depths, the doping of the source/drain structures needs to increase beyond current solid solubility limits. In order to continue this decreasing trend, it becomes increasingly important to understand and control the solid solubility and the diffusion of dopants in silicon. The ability to accomplish this will depend on our understanding of how dopants and silicon interstitials interact. This chapter will approach the more fundamental issue of how arsenic and silicon interstitials interact in reference to the release of silicon interstitials.

CVD grown boron marker layers were used to monitor the release of silicon interstitials from an arsenic doped surface region that was subsequently implanted with silicon. These structures were annealed for

various times at 750°C in an ambient of nitrogen. A comparison of boron spike enhancement and defect dissolution is made. It is shown that enhancement values from the silicon implant were reduced at short times for samples containing arsenic compared to samples implanted with silicon alone or arsenic alone. The TEM results showed that defect densities were dramatically reduced for the samples containing arsenic. These results imply that the previously reported reduction in {311} formation observed in As doped wells is most likely not a Fermi level effect and is consistent with the formation of As interstitial complexes. The data shows that As-I complexes form, and control extended defect formation, which slows the enhanced diffusion.

3.1.2 Boron Marker Layer Setup

Boron marker layers can be used to study the release of interstitials from an implanted region. The release of interstitials from the implanted region will subsequently enhance the motion of a buried boron marker layer. The motion of the marker can be used to determine an enhancement value over that of inert diffusion and the enhancement can be monitored over a range of times and temperatures. Figure 3.1 is an example of a boron marker layer sample after annealing showing the difference between inert and enhanced diffusion. TEM samples can also be made from these samples to compare the release of the motion of the

boron spike with the dissolution of extended defects. This information will help in determining whether the diffusion enhancement comes from the extended defects or from other submicroscopic clusters such as arsenic-interstitial clusters.

3.1.3 Special Considerations for Implant Conditions

A variety of implants involving arsenic and silicon can be used in conjunction with the boron marker layers to observe the arsenic-interstitial interaction. Special considerations must be taken when selecting the implant conditions for the arsenic and silicon. The arsenic implant must be of sufficient concentration such that no extended defects form during the annealing of the silicon implant. However, the arsenic concentration should not be of such high concentration that interstitial injection occurs from As_4V cluster formation[49-51,63-65]. The silicon implant needs to be of an energy such that the entire silicon implant profile is contained within the arsenic profile. The dose should also be adjusted such that there is sufficient arsenic-interstitial combination without forming extended defects or an amorphous layer.

The enhancement values, $\langle D_B \rangle / D_B^*$, can be extracted using the following procedure. After annealing, the boron profiles can be measured by secondary ion mass spectrometry (SIMS). The initial and final profiles

obtained by SIMS can be imported into FLOOPS and a simulated diffusion can be run assuming an inert diffusion coefficient, until the annealed profile is obtained. The time averaged diffusion coefficient is equal to the diffusive broadening over the total anneal time,

$$\langle D_B \rangle = \frac{\int_0^t D(t)dt}{t} \tag{3.1}.$$

Using an accepted value for the boron diffusion coefficient and diffusing over an enhanced time, t_{enh}, equation 3.1 is reduced to,

$$\langle D_B \rangle = \frac{D_B^* t_{enh}}{t_{ann}} \tag{3.2}.$$

Rearranging equation 3.2 shows that the ratio of the enhanced anneal time to the actual anneal time is directly proportional to the ratio of the time averaged diffusion coefficient to the inert diffusion coefficient,

$$\frac{t_{enh}}{t_{ann}} = \frac{\langle D_B \rangle}{D_B^*} \tag{3.3}.$$

If arsenic is acting as a trap for the silicon interstitials in some way, then there should be a difference in diffusion enhancements when comparing profiles from the arsenic only, silicon only, and arsenic plus silicon samples. If arsenic is not affecting the silicon interstitials then no difference between the profiles should be observed. The result of the comparisons between the different implant samples can provide the

information necessary to establish the nature of the defect controlling the enhanced movement of the boron marker layer.

The observed enhancement can manifest itself in many ways. If the effect was purely a Fermi level dependence, then one would expect more of an enhancement from the arsenic plus silicon case over that of the silicon alone case. In the case of arsenic trapping interstitials, one would expect the enhancement of the arsenic plus silicon to be slowed at first and then when the arsenic clusters begin to break up an increased enhancement would follow. In the event that the arsenic doesn't interact with the interstitials, there would be no difference in any profile at any stage of annealing.

3.2 Experimental Overview

Boron spikes with a peak concentration of $2x10^{18}$ cm^{-3} were CVD grown in silicon wafers. The maximum boron concentration occurred at a depth of 4500 Å. Arsenic was then implanted at 3keV and a dose of $1x10^{15}cm^{-2}$. Following the implant wafers were RTA annealed at 1050°C for 15sec. The goal of the arsenic implant and anneal was to create an active arsenic profile with very little end of range damage (EOR) and a junction depth of about 1000 Å. Following the RTA anneal, pieces of the wafer were implanted with silicon at 25 keV and a dose of $1x10^{14}$ cm^{-2}.

Control wafers with no arsenic or silicon implant were fabricated for comparison. All wafers were subjected to the RTA anneal, before the silicon implant, so that the same thermal budget was used in all cases. Each wafer was subsequently annealed at 750°C for times ranging from 5 min to 360 min in a nitrogen ambient furnace. Table 3.1 is a summary of the different process steps of each type of sample. Figure 3.2 is a schematic view of the wafer processing steps.

Table 3.1. Different process steps used in the boron marker layer study.

Process	As implant	RTA	Si Implant	750°C anneal
A	No	Yes	Yes	Yes
B	Yes	Yes	Yes	Yes
C	Yes	Yes	No	Yes

Secondary Ion Mass Spectroscopy (SIMS) was performed on a CAMECA 3F to monitor the motion of the boron spike. The profiles were obtained using an O2 beam at an energy of 5.5 keV and raster area of 250 μm x 250 μm. The beam current was set to approximately 200 nA which gave a sputter rate of 5±0.5 Å/sec. After SIMS analysis, the crater depths were measured with a stylus profilometer with a diamond tip. Depths were measured across each direction and averaged for calculation of the crater depth. Gaussian curves were then fit to the measured profile using the Excel macro described in Appendix A. Time averaged

enhancement values $\langle D_B \rangle / D_B^*$ of the boron spike were then extracted assuming the inert diffusion of boron at 750°C is 2.69×10^{-18} cm^2/sec.[80] TEM samples were also made from the selected samples after SIMS analysis as stated in chapter 2.

Figure 3.3 is a combination of SIMS plots for a series of the control samples. Spike A is the as grown boron spike before any processing. Spike B is the as grown spike after an RTA anneal at 1050°C for 15 sec. A Gaussian fit to this curve is also presented to demonstrate the accuracy of the fit that was used. In all cases the fitting parameter, R, was equal to 0.98 or more, with R=1 being a perfect fit. The final spike, C, is the SIMS data after the arsenic implant and RTA annealing. The profiles after RTA in the arsenic implanted and RTA annealed samples showed no additional motion in the boron marker layer, within SIMS error, compared to that of the as grown sample plus RTA. Spike B was used as the initial spike in determining time averaged enhancement values in all cases.

3.3 Results and Discussion

Figure 3.4 is a plot of the total time averaged enhancements versus time for sample sets A, B, and C. Transmission Electron Microscopy (TEM) of the 15 minute samples showed a high density of

{311} defects for the silicon implanted samples without arsenic. No defects were observed for the arsenic plus silicon samples, which is consistent with previous studies [44]. The 360 minute samples showed no defects in either case. Silicon implanted samples showed the greatest enhancement in all cases. Samples implanted with arsenic alone appear to be above the clustering limit and, therefore, exhibit interstitial injection through a vacancy clustering reaction as shown in earlier studies by Rousseau [50]. The interesting case is when the arsenic background is implanted with silicon. One would expect that when the implant damage associated with the arsenic implant is combined with the implant damage from the silicon implant that there would be an additive effect and a large amount of diffusion enhancement would be observed. As shown in Figure 3.4 this is not the case. When the implants are combined there is less motion than for either of the single implants for short times.

The data in Figure 3.4 implies that there is some sort of pair reaction associated with the arsenic and silicon and this pair is stable for short times. A counter argument is that the effect is the result of a change in the Fermi level. One possibility is because the charged vacancy is believed to have a higher diffusivity and they diffuse away and reduce the supersaturation before {311}'s can nucleate[74]. However, this would imply the spike shows a greater diffusivity not less, thus As-I pairs appear

to be the most plausible model at this time. Once the pair begins to break up the diffusion enhancement is similar to that of the silicon alone case, but there is still less net interstitials available for motion of the boron spike. The data also seems to indicate that the addition of silicon interstitials is slowing the arsenic/vacancy clustering reaction. This is apparent through the delay in enhancement values at short times.

An arbitrary line with a slope of –1.0 was added to Figure 3.4 to show what the slope of the enhancement curves would be if all interstitial injection were completed. The slope approaches minus one when the diffusion enhancement approaches a value of t^{-1}. The final portions of the enhancement curves have slopes of -0.75 for the silicon and arsenic/silicon samples and a -0.91 slope for the arsenic alone sample, which shows that there is still some interstitial injection even after long time anneals.

3.4 Boron Marker Layer Summary

Boron marker layers were used to study the release of interstitials from an arsenic well with implants of silicon. It was shown that for short times the arsenic plus silicon implants exhibited less diffusion than a single implant of arsenic or silicon. TEM images showed a high density of {311} defects for the silicon alone case and no defects for the arsenic

implanted sample both after RTA and after a subsequent Si implant and low temperature annealing. The delayed release of interstitials and the lack of extended defects is consistent with arsenic trapping the excess interstitials through an As-I type complex formation and these pairs appear to be less stable than {311} defects.

3.5 Antimony Doped Superlattices

As the semiconductor community continues to decrease the size of the transistor to smaller and smaller dimensions, issues of dopant diffusion and dopant activation become some of the major concerns. Arsenic is generally used as an n-type dopant in silicon due to its high solubility and low diffusivity. Even though arsenic displays these desirable qualities, the increased demands are pushing the limits of its usefulness. [1] The regions with arsenic doping are generally at concentrations that exceed the solid solubility limit in silicon. It has been shown in previous studies that exceeding the solubility limit presents many problems in silicon.[50,58,81] Recent studies by Jones *et al.*[82] have shown that at low energies and moderate doses, arsenic displays dramatic transient enhanced diffusion (TED) effects after anneals at 750°C while no evidence of extended defects are found. Since arsenic is known to diffuse by a dual mechanism involving interstitials and vacancies,[29] the

TED effects were suggested to be due to the formation of mobile arsenic-interstitial complexes or a vacancy release upon monoclinic SiAs precipitate formation.[83-85] These explanations are possible due to the different stages of arsenic-defect interactions available as the arsenic concentration is increased.

At low arsenic concentrations (< $1x10^{20}cm^{-3}$) arsenic has been shown to affect interstitial populations by forming arsenic-interstitial complexes.[44,45] As the arsenic concentration is increased, arsenic-vacancy clusters begin to form and eventually a concentration is reached where SiAs precipitates form.[54,55,61,62,66,69,86,87] It has been suggested that the formation of SiAs precipitates occurs through the combining of arsenic-vacancy clusters.[16] When the clusters combine they would inject a vacancy into the bulk. This could cause the reduction of interstitial rich extended defects or in the motion of the arsenic profile. A recent study reports the effect of interstitial injection from low energy, moderate dose arsenic implants on the motion of a boron marker layer (to be published in Spring MRS 2001 Proceedings). It was found that at lower concentrations interstitial injection was not inhibited, but at higher arsenic concentrations all interstitial injection ceased. It was suggested that vacancies injected from the precipitation process could have effected the interstitial population and effected both the interstitial

injection and the formation of extended defects in the end of range. In this article the injection of vacancies from arsenic implanted regions will be explored.

3.5.1 Antimony Experimental Setup

Doping superlattices (DSLs) with six spikes of $1x10^{14}$ cm^{-2} antimony were grown on a Si(100) substrate by a custom-made MBE system, with growth details described previously.[88] The antimony spikes were grown 10nm in width with the peak centers spaced 100nm apart. The shallowest spike was capped with 50nm of silicon. The silicon regions were grown at 450 °C, while the regions containing antimony were grown at 230 °C followed by a 650 °C 120 sec rapid thermal anneal after the completion of each spike layer. Three samples were implanted with arsenic at 3 keV to doses of $5x10^{14}$, $1x10^{15}$, and $5x10^{15}$ cm^{-2}, respectively. The implanted samples were furnace annealed at 750 °C for 4 hr, followed by a second furnace annealed at 800 °C for 1 hr. An unimplanted sample underwent identical processing steps. Secondary ion mass spectroscopy (SIMS) analysis was performed on all samples using a Physical Electronics ADEPT-1010 system to determine the antimony and arsenic concentration versus depth profiles before and after annealing. Arsenic and antimony were monitored as negative molecular ions, $AsSi^-$ and $121SbSi^-$, under Cs^+ bombardment at an energy of 1 keV and an

angle of 60°. Secondary ions were collected from the center 3% of a 450 x 450 μm rastered area. Stylus profilometry was used to determine the depth of the sputtered craters. The atomic concentrations of arsenic and antimony were calculated from relative sensitivity factors determined from standard samples. The depth scale of the antimony profiles after annealing was laterally shifted no more than 20 nm (within one standard deviation, estimated at 0.05, in relative depth scale error of SIMS[89]) so that the peaks aligned with those of the as grown profile. The antimony concentration scale of the annealed profiles was standardized by equalizing the total dosage in each peak to that of the as grown profile.

3.5.2 Vacancy Injection From Arsenic Doped Layers

The goal of this experiment was to examine any vacancy injection upon the formation of SiAs precipitates. Antimony is known to diffuse mainly by a vacancy mechanism.[29] Therefore, if antimony marker layers are present below the surface, the enhanced motion of the marker layer would serve to monitor vacancy injection into the bulk. The low energy implants were performed to ensure the absence of end of range (EOR) defects, while using doses known to be located in the clustering and precipitation regimes. With no extended defect formation and the use of clustering/precipitation type doses, the enhancement of the antimony

marker layers should be solely an effect of the clustering/precipitation process.

Figure 3.5 shows the SIMS results for the arsenic implanted regions before and after annealing at 800°C for 1 hr. The peak concentrations are such that clustering and precipitation should occur for the conditions used. Figure 3.6 is a plot of the arsenic clustering and precipitation regions determined by Solmi *et al.*[87], and Derdour *et al.*[90] with the peak doses of the implants used in this study included before annealing. An indication that clustering and precipitation are occurring in these samples are the kinks in the profiles in Figure 3.5 around arsenic concentrations of $1x10^{19}$ for the lower dose and $1x10^{21}$ cm^{-3} in the higher dose case. These concentrations are in agreement with the clustering and precipitation limit at this annealing temperature. The additional motion in the higher dose case at higher concentrations is believed to be from the formation of the As_nV clusters mentioned in Chapter 1. If this were the case the clusters would need to be in a mobile form and it has been shown by Uematsu et al.[91] that indeed a having mobile As_2V cluster can help to explain high concentration arsenic diffusion. Simulations of these profiles are presented and discussed in Chapter 4. With the effects seen in the SIMS profiles that are consistent with high concentration arsenic effects after annealing it is believed that the formation of precipitates occur in the

highest dose samples and clusters in the lower dose. Therefore, after annealing it is expected that if there were any vacancy injection from these processes, an enhancement in the antimony layers would be observed.

After the 750°C 4 hr anneal, no enhanced motion was seen in the antimony spikes. The lack of motion was attributed to the low diffusion coefficient of antimony in silicon. Even though no enhanced diffusion was observed, the initial anneal did ensure the annihilation of any EOR interstitials during regrowth of the arsenic implanted region.

A subsequent 800°C 1hr anneal was performed and the arsenic and antimony spikes were once again monitored. In addition to the as-implanted profiles, Figure 3.5 also presents the arsenic profiles after the second annealing cycle. As discussed previously the hump in the EOR region is evidence that precipitation and clustering occurred during the annealing cycles. Figure 3.7 shows the first of the antimony spikes before and after arsenic implantation and annealing. As was seen in the first annealing cycle at 750°C there is no measurable diffusion enhancement of the antimony spikes after annealing. All the spikes in each sample moved the same amount, therefore the initial spike in each sample is only shown to enhance the effect or lack there of. The motion that was recorded was modeled using Florida's Object Oriented Process

Simulator (FLOOPS). It was found that even though there was no enhancement due to the arsenic implants, there was still an overall diffusion enhancement of about 150X. The exact nature of this enhancement is not known at the time of this publication, but may be due to grown in defects or impurity elements. Whatever the case, Figure 3.7 shows that no additional enhancement was observed after arsenic implantation and annealing. This indicates that there is no measurable injection of vacancies due to the clustering or precipitation processes at low implant energies. This is consistent with higher energy and dose arsenic implants studied by Venables *et al.*[17]

The results of this experiment show that the antimony marker layers are unaffected by the clustering and/or precipitation process. There are a number of reasons for the experimentally obtained results. Due to the low implant energy, the arsenic profile is initially contained within the first 10nm of the surface. It is possible that any vacancy flux is annihilated by recombination at the surface. Previous investigations of MeV and medium energy implantation into antimony structures have shown that vacancies formed in the near surface region do indeed diffuse into the bulk in concentrations significant enough to cause antimony diffusion.[92,93] Therefore, vacancies can travel into the bulk from the implanted region, but whether there is a sufficient flux of vacancies to

cause enhanced diffusion is unknown at this point. Another possibility is that clusters consisting of As_nV release m arsenic atoms, not vacancies, to form $As_{n-m}V$ complexes upon precipitation. Regardless of the exact explanation, the absence of enhanced diffusion of the marker layers indicates that vacancy injection into the bulk is immeasurable upon precipitation.

The results of this experiment also eliminate possible explanations used in other experiments. For instance, the possibility of vacancies eliminating the extended defects in the EOR region may be discounted. It appears that the interstitials that make up the extended defects prefer to go to arsenic atoms and form arsenic-interstitial complexes during the initial stages of the annealing cycle. Since no vacancy injection results from annealing, the arsenic-interstitial interaction seems to be the controlling factor.

3.5.3 Antimony Doped Superlattice Summary

The injection of vacancies from arsenic implanted regions was studied using antimony doped super-lattice structures. It was found that after arsenic implantation and annealing there was no enhanced motion in the antimony spikes compared to unimplanted samples. This result indicates that no vacancies were injected due to the formation of monoclinic SiAs precipitates. It also showed that vacancy injection is not

the reason for reduced extended defect formation in the EOR regions associated with low energy arsenic implantation. It is therefore thought that the arsenic-interstitial complex formation is the main contributor to the elimination of defects below 4 keV.

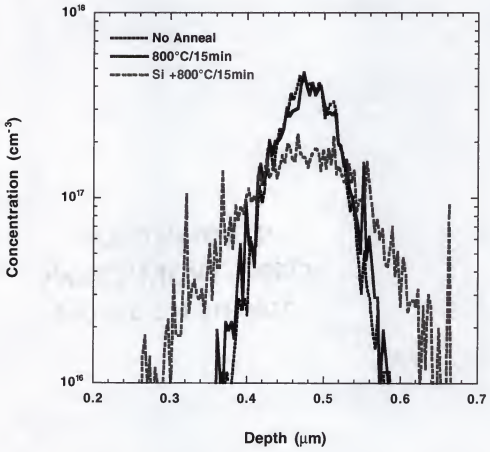

Figure 3.1. Example of the difference between inert and enhanced diffusion at 800°C 15 min. The sample with the silicon implanted shows greater diffusion after annealing compared to a sample with no implant.

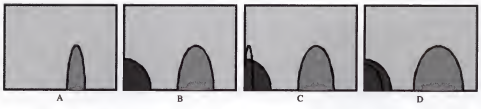

Figure 3.2. Fabrication process for boron marker layer experiment. A) Boron spike grown by CVD. B) Implant arsenic at 3keV, $5x10^{14}$ cm^{-2} and anneal in a RTA at 1050°C for 15 sec to produce a 1000Å junction depth. C) Implant silicon at 25keV, $1x10^{14}$ cm^{-2}. D) Anneal in nitrogen ambient at various temperatures and times. Control wafers are made using the same process minus the arsenic step.

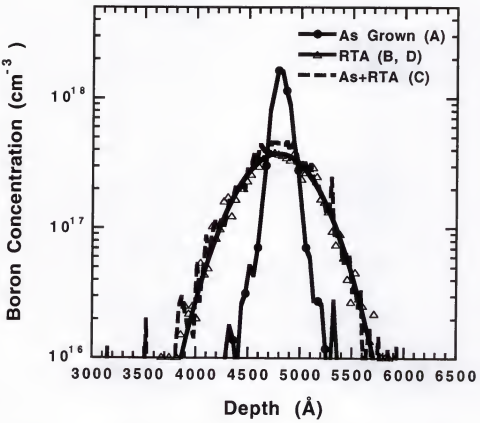

Figure 3.3. Secondary Ion Mass Spectroscopy (SIMS) plots of from A) the as grown spike, B) non-implanted spike after RTA, C) after arsenic implant and RTA and D) a gaussian fit to the non-implanted plus RTA data.

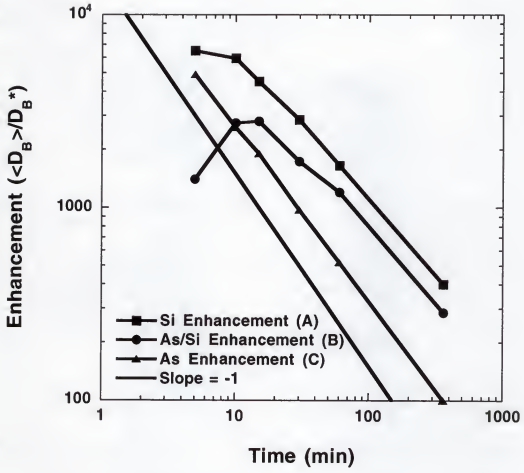

Figure 3.4. Time averaged enhancements versus time for samples annealed at 750°C in a nitrogen ambient.

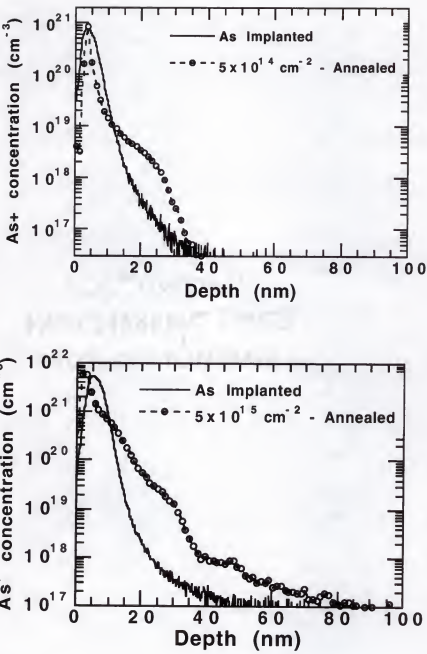

Figure 3.5. SIMS arsenic concentration profiles as implanted and after anneal in N_2 at 800 °C for 1 hr for 3 keV (a) $5x10^{14}$ cm^{-2} and (b) $5x10^{15}$ cm^{-2} arsenic implanted samples.

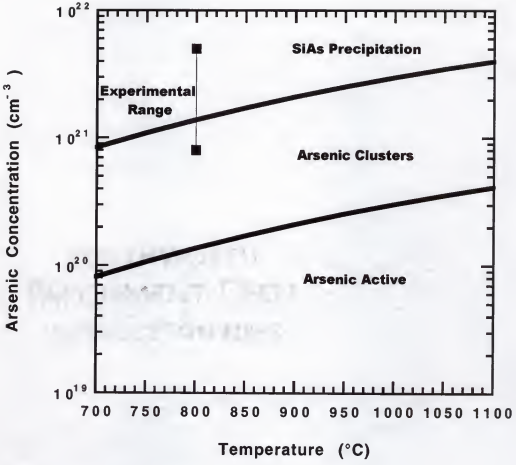

Figure 3.6. Location of the peak profiles with respect to the projected clustering and precipitation ranges. The higher doses lead to precipitation where the lower dose leads to clustering.

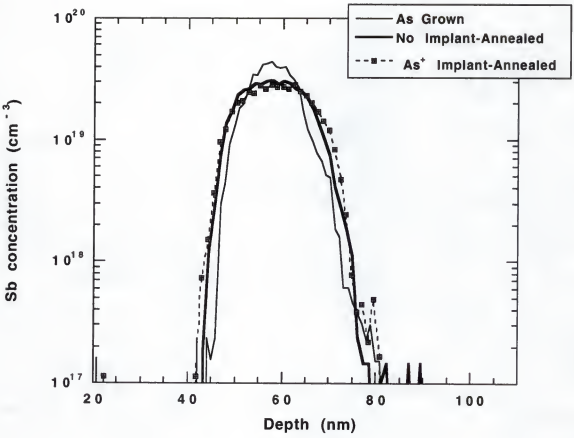

Figure 3.7. SIMS antimony concentration profiles for the shallowest peak of the antimony DSL as grown and after anneal in N_2 at 800 °C for 1 hr for both the no implant and 3 keV $5x10^{15}$ cm^{-2} arsenic implant samples. The implanted profile exhibits no enhanced diffusion.

CHAPTER 4
MODELING

4.1 {311} Defect Dissolution Model

In earlier chapters emphasis was placed on the experimental aspects of arsenic-silicon interstitial interactions. These results are most useful when they can be molded into models for use in process simulation software. In this way future devices can be designed such that the arsenic-interstitial interaction can be taken into account when appropriate.

Recently, Law *et al.*[94] developed a {311} model that predicts the formation and dissolution of {311} defects in silicon. This model has been implemented within the Florida Object Oriented Process Simulator (FLOOPS) and with a few additions the arsenic-interstitial interaction can be included in the model. The simplest way to begin to model the As-I interaction is to begin with a basic pair reaction. In this form the arsenic-interstitial reaction is treated as follows,

$$As + Si_{(I)} \Leftrightarrow AsI \tag{4.1}$$

This reaction can be modeled in FLOOPS using an equation of the following form,

$$C_{AsI} = C_I * C_{As} \frac{\exp\left[\frac{E_b}{kT}\right]}{5x10^{22}} \tag{4.2}$$

C_{AsI} is the concentration of arsenic pairs, C_I is the concentration of interstitials added from damage of a silicon implant, C_{As} is the arsenic background concentration, E_b is the arsenic-interstitial binding energy, k is Boltzman's constant, T is temperature in Kelvin and $5x10^{22}$ (cm^{-3}) is the concentration of atoms in the silicon lattice. A self-implant of silicon at 40kev, $1x10^{14}$ cm^{-2} was simulated with UTMARLOWE in order to determine C_I. The damage profile is the same for all models in this study at time zero. If other energies or doses of silicon were to be simulated, a new damage profile would need to be formulated.

The first step in developing the model is to simulate a few parameters to check the validity of the equation. In Chapter 2 the arsenic-interstitial interaction was shown to affect the number of defects that nucleated but not affect the dissolution of those defects. Figure 4.1 is a comparison between experimental data obtained at 750°C and a simulation of the same condition. From this figure it seems that the dissolution rates are not consistent. The dissolution rate is known to be

inconsistent from experiment to experiment depending on a number of parameters such as ion implantation source, furnace type, starting material, etc. The exact reason for the difference has not been determined at this time. Experimental data obtained from various experimental sources are presented in Figure 4.2 for similar implant and annealing conditions.[32,39,44,78,79,95-97]

A simple solution to the discrepancy shown in Figure 4.1 is to adjust the simulation temperature. Since the dissolution is exponentially dependent any change in temperature will effect the slope of the curve profoundly. Figure 4.3 is a plot of the low concentration arsenic simulation that has been adjusted by 15°C. With the simple adjustment, the dissolution rate difference has been corrected and direct comparisons can be made. Figure 4.3 also includes the simulation for $3x10^{17}cm^{-3}$ arsenic that determines the low arsenic concentration sample to be comparable to the control sample. The majority of the difference in magnitude between the data and simulations may be attributed to statistical counting variations. Another possibility is that the initial damage profile may not be equal to the experimental damage profile. A slight adjustment may be made to the damage profile if the same adjustment is made throughout the entire modeling effort in a single experiment. In this set of simulations there was no adjustment made to

the initial damage profile. The important parameters to match are the percent change in the zero time interstitial profile and the slope of the dissolution.

4.2 Process Simulation

4.2.1 Arsenic Interstitial Binding Energy Determination

A second test for the use of Equation 4.1 in the pair model is to test the binding energy dependence on the time zero trapped interstitials. A simulation illustrating the effect of changing the binding energy on a high arsenic concentration sample is presented in Figure 4.4. The addition of arsenic to the system is observed to lower the initial starting point for the {311} dissolution. This is consistent with observations presented in Chapter 2. A feel for the validity of the model is also beginning to take shape. Not only is a drop in time zero trapped interstitials seen, but once the defects are nucleated there is no effect of arsenic upon their dissolution. This is the same phenomenon is seen in the experimental data presented in Chapter 2.

To determine the binding energy used in the model a number of simulations were run. Presented in Figure 4.5 are the results of several simulations at different binding energies. The time zero trapped interstitial values were extracted from 750°C dissolution simulations with

various arsenic background concentrations. When compared to 750°C experimental data, presented in the same figure, the important parameter is how much the trapped interstitial value at zero time decreases at each concentration. When this parameter is taken into account then 0.95 eV looks to fit the best in each case. Another way to see the fit is to look at the percent decrease at each concentration when normalized to a particular concentration. Figure 4.6 shows the percent decrease in the trapped interstitials at zero time when the curves are normalized to an arsenic concentration of $3x10^{17}$ cm^{-3}. When taking the error bars into account the binding energy that gives the best percent decrease at each concentration studied is 0.95 eV. The binding energy calculation was determined at a temperature of 750°C and fits well with experimental data, however this model must also work across the range of temperatures used in this study.

4.2.2 Temperature Dependence of Simulations

A single binding energy should produce the same value of trapped interstitials at zero time independent of temperature. A temperature independent As-I binding energy implies that the arsenic is paring with interstitials during the initial stages of annealing. With a number of the interstitials involved in pairing reactions there are less interstitials available for {311} nucleation. The temperature dependence of the time

zero trapped interstitials are plotted in Figure 4.7. As expected there is no temperature dependence in the simulations or experimental data. To further illustrate that a single binding energy may be used for all studied cases, the trapped interstitials at zero time are plotted in Figure 4.8 as a function of arsenic concentration for each temperature.

4.2.3 Simulated Results

With all of the preliminary steps completed and satisfied the model can be used to predict the behavior seen experimentally. The first related simulation is to run the $3x10^{17}$ cm^{-3} arsenic concentration simulations. This simulation has very little arsenic and therefore should match with little error. Presented in Figure 4.9 are the experimental data and simulated results for $3x10^{17}$ cm^{-3} arsenic wells. As expected, for all temperatures studied, the simulations are very good. Figure 4.10 and 4.11 present the same fits for $3x10^{18}$ and $3x10^{19}$ cm^{-3} arsenic concentrations, respectively. In these simulations, the fits are good at the higher temperatures of 750°C and 800°C. However, at lower temperatures the simulations exhibit greater error.

This may to be due to one of several effects. First, the {311} defects at 700°C are extremely difficult to count due to their small size. Referring to Figure 2.4 it is plausible that there is more error associated with the counts than is commonly stated. Secondly, recalling studies

from the high arsenic concentrations presented in Chapter 1, arsenic begins to go to clustering reactions at approximately $8x10^{19}$ cm^{-3}. The simulations at high concentrations and low temperatures represent a "worst case scenario" when nucleation of a second phase is considered. It is possible that at the higher concentrations the experimental results are reaching into an alternate defect regime and a simple pair model is no longer applicable.

4.3 Using the As-I Pair Model for Testing Ramp Rate Effects

It was stated in the previous section that the interstitials were pairing in the initial stages of the annealing cycle. The {311} model in FLOOPS has a barrier to {311} formation of 0.5 eV where the As-I pair has no barrier to formation. This allows the As-I pairs to form via a diffusion limited reaction while {311} formation must overcome the 0.5 eV energy barrier. The net effect at short times is that there are less interstitials available for {311} nucleation. Once the barrier is reached the interstitials will preferentially fall into the {311} defect sites. This is the cause of the lower time zero trapped interstitial value at increased arsenic concentrations. With an increase in arsenic atoms, the interstitials available for {311} formation is decreased which leads to a lower zero time value.

Since the interstitials are believed to pair at the initial stages of annealing, increasing the ramp rate should cause an increase in the number of interstitials available for {311} formation. At increased ramp rates there would be less time spent in the pair regime before the {311} nucleation barrier was crossed. Presented in Figure 4.13 is the simulated result of what happens when the ramp rate is increased. As expected the higher ramp rate causes the number of As-I pairs to decrease and therefore, the number of interstitials at zero time is increased. Experimental results to prove the simulations are presented as future experiments.

4.4 Modeling of High Concentration, Low Energy Arsenic

Experimental results presented in Chapter 3 have shown that there is enhanced diffusion in the arsenic profiles (Figure 3.5) when annealed at 800°C for 1 hr. Also, in previous experiments by Jones et al.[82] it was suggested that interstitials present at the end of range were responsible for a lack of extended defects. To test this theory and predictions of the enhanced diffusion, the As-I pair formation model was applied to low energy, high dose simulations.

Arsenic implants were simulated using UTMARLOWE 5.0 to determine the as-implanted profiles for the arsenic, interstitials and vacancies for 3 keV implants. The simulated implant doses were $5x10^{14}$,

$1x10^{15}$ and $5x10^{15}$ cm^{-2}. In order to obtain the correct interstitial profiles the initial damage profiles were truncated to the amorphous depth. In this manner only the interstitials near the end of range will be responsible for observed effects. The results after simulation are compared to the SIMS profiles of the low energy arsenic presented in Figure 3.5.

To determine if any defects form the {311} model was included in all simulations. Figure 4.14 shows the difference in the $1x10^{15}$ cm^{-2} defect profiles with and without arsenic present. What is significant is that when arsenic is present no defects form. This is in direct correlation with experimental results and the experiments presented in Chapter 2. However, as can be seen in Figure 4.15, there is no effect on the diffusion with the inherent pair model. This was mainly due to the fact that there is no diffusion associated with the As-I pair in FLOOPS. The inherent values are set to diffuse by vacancy mechanisms alone. Because there was a room temperature pre-anneal, and the vacancies are assumed to have an enormous diffusivity even at room temperature, no significant population of vacancies is observed.

The total diffusion of arsenic with interstitials is described by

$$D_{ASI} = D_0 + \frac{n}{n_i}\left(D_n\right) + \ldots \tag{4.3}$$

where

$$D_0(T) = D_0 \exp\left(\frac{-E_a}{kT}\right) \tag{4.4}$$

$$D_n(T) = D_n \exp\left(\frac{-E_a}{kT}\right) \tag{4.5}.$$

As was mentioned previously, the diffusion coefficients for D_0 and D_n are set at 0, therefore there is no diffusion by interstitials accounted for in FLOOPS. As presented in Figure 4.15, the diffusion is greatly underestimated with these values when low energy high dose arsenic implants are annealed at 800°C for 1 hr. By allowing the arsenic to begin to diffuse with interstitials the simulations begin to resemble the diffusion seen experimentally. *Ab initio* calculations and previous studies have shown the activation energy of the As-I system to be ~4.2 eV.[91,98-100] The n/n_i factor causes D_n to affect high concentration portions of the profiles. D_0 will have an effect at lower concentrations. Adjusting the pre-exponential term in both equations will allow the shape of the profiles to be adjusted accordingly. Presented in Figure 4.16 is the simulation results when diffusion by interstitials is accounted for. The values used for each term in each equation are presented in Table 4.1. The simulation at this point has a good overall fit. A possible concern with this model is that no clustering effects are included. Studies have shown, that at high concentration, clustering and precipitation effects will contribute to the diffusion.[18,46,47,50,87] Figure 4.17 presents the simulation results of a 3

keV, $5x10^{15}$ cm^{-2} arsenic implant which has been annealed at 800°C for 1 hr. At this concentration the diffusion is severely underestimated which is most likely due to neglecting the clustering and precipitation effects. This modeling work demonstrates the need to include the As-I interaction and diffusion based on the interstitials. Suggested future work would be to include clustering effects and possibly a concentration dependent factor such that a single model can be used for all concentrations of arsenic.

Table 4.1. Parameters used in As-I simulations

Equation	Equation Type	Pre-exponential	E_a
As-I	Arrhenius	$8.023x10^{23}$	-1.0 eV
D_0	Arrhenius	10.0	4.2 eV
D_n	Arrhenius	1.0	4.2 eV

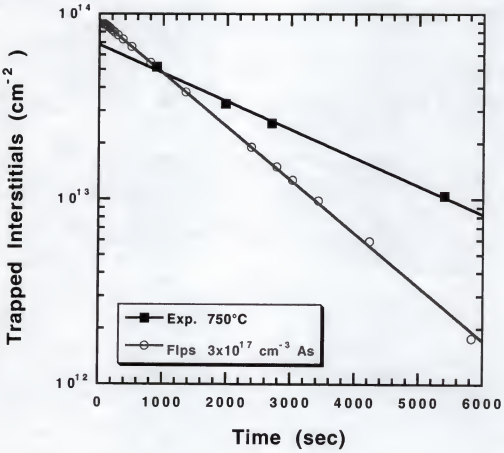

Figure 4.1. Difference in FLOOPS simulations and experimental data for {311} dissolution. The difference in decay constants comes from a variation ion furnace temperature. The slope difference can be adjusted be a slight temperature adjustment in the simulations as shown in Figure 4.3.

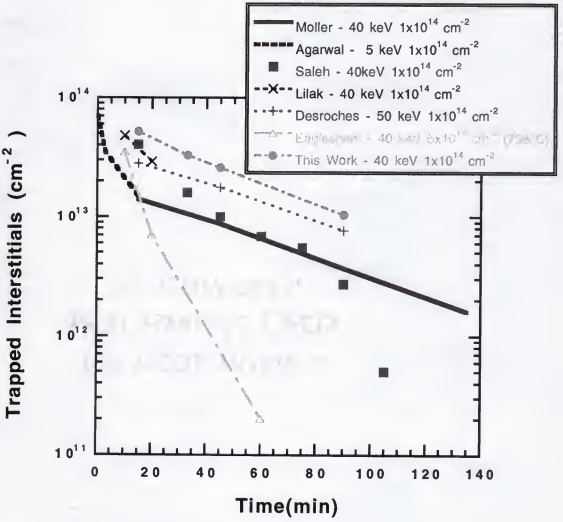

Figure 4.2. Scatter of different data from published sources on {311} dissolution rates. The scatter shows that the time constants vary anywhere from 10 to 55 minutes. The data collected in this experiment fits in around the 50 min mark.

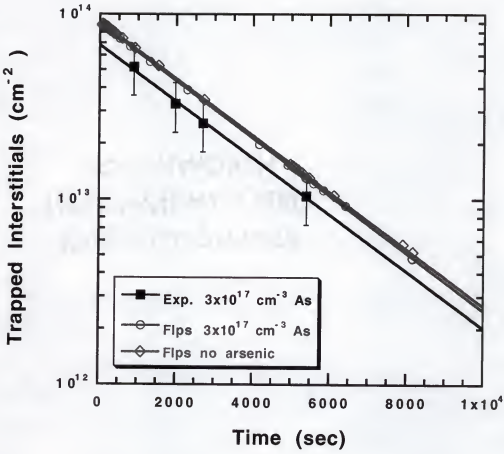

Figure 4.3. Dissolution curves at 750°c for an arsenic concentration of $3x10^{17}$ cm^{-3}. The simulations show that there is no effect from arsenic until after the concentrations exceed concentrations of $3x10^{17}$ cm^{-3}, therefore $3x10^{17}$ cm^{-3} can be considered to be a control sample. Also shown in this plot, is that with a slight temperature correction the experimental data and simulations show similar slopes. This temperature correction is warranted due to the large scatter in published data.

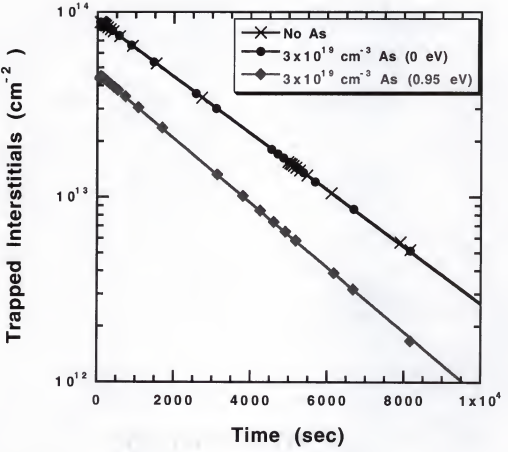

Figure 4.4. Effect of changing the binding energy on the dissolution curves. With a binding energy of zero, there is no effect from the arsenic. When the binding energy is increased an effect begins to be noticed. As with experimental results there is no change in the dissolution kinetics. This seems to imply that arsenic is having the biggest effect at the initial stages of annealing before extended defects nucleate.

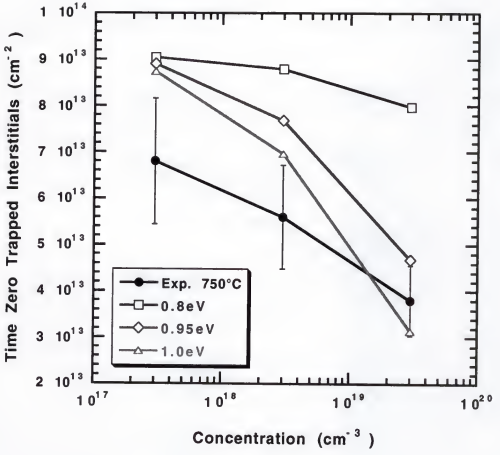

Figure 4.5. Effect of changing the binding energy on the trapped interstitials at time zero. The important point is that similar shapes are seen between the data and a binding energy of 0.95 eV.

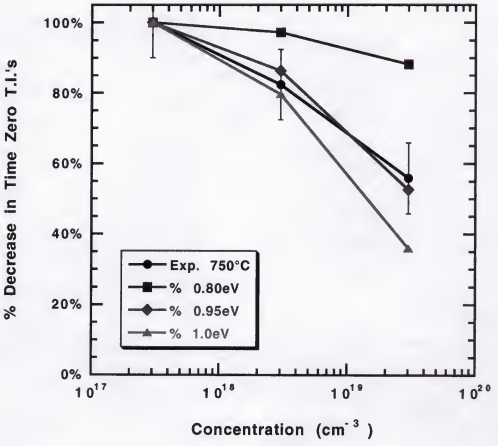

Figure 4.6. Effect of changing the binding energy, expressed as a percent drop in the number of trapped interstitials at time zero. A good fit to the data is seen for a binding energy of 0.95 eV.

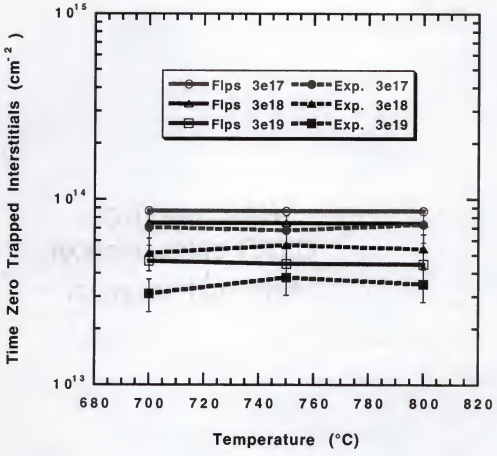

Figure 4.7. Effect of temperature on the number of trapped interstitials at time zero. Having no dependence relays that the time zero trapped interstitial value is related to the implant conditions and the initial stages of the annealing cycle.

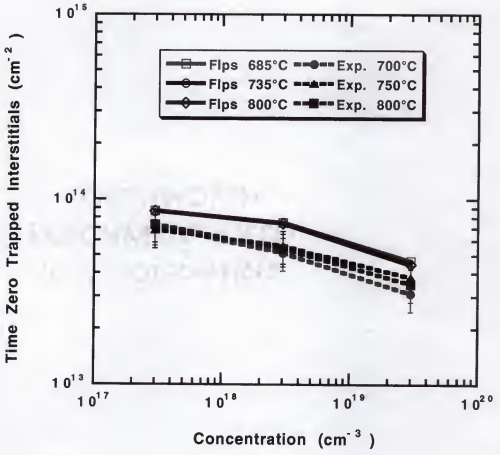

Figure 4.8. Plot of the number of trapped interstitials at zero time as a function of arsenic concentration. This figure shows that with a single binding energy the same reduction with respect to the arsenic concentration is seen at all temperatures.

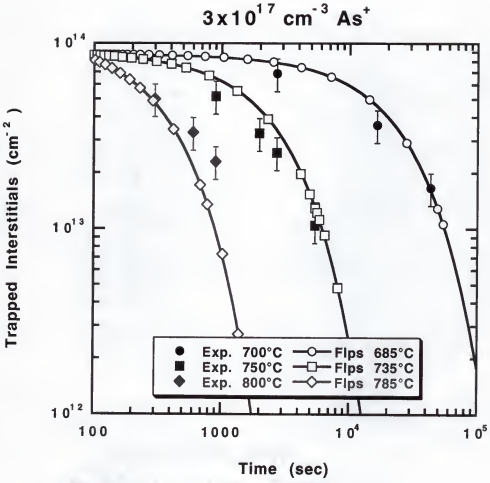

Figure 4.9. Simulation runs versus experimental data at an arsenic concentration of $3x10^{17}$ cm^{-3}. At these concentrations arsenic has little effect on the dissolution, therefore good fits are expected and obtained.

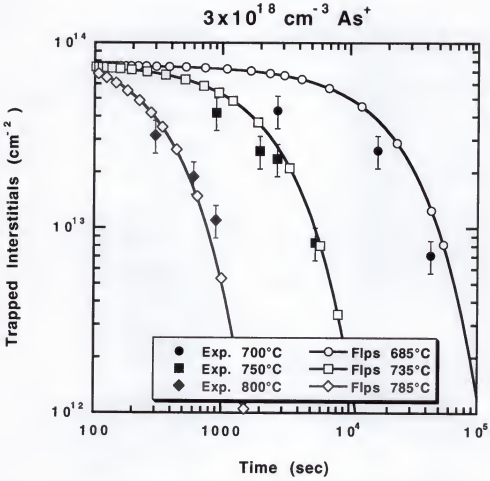

Figure 4.10. Simulation runs versus experimental data at an arsenic concentration of $3x10^{18}$ cm^{-3}. Good fits are realized at all temperatures studied

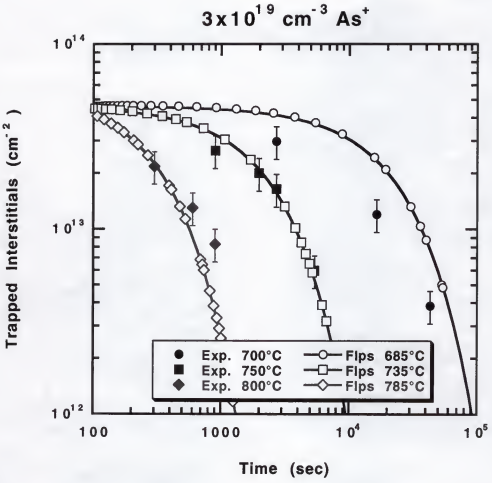

Figure 4.11. Simulation runs versus experimental data at an arsenic concentration of $3x10^{19}$ cm^{-3}. Good fits are seen for the higher temperatures. At 700°C it is speculated that high arsenic concentration effects are beginning to play a role in the dissolution and a more complicated model may be needed.

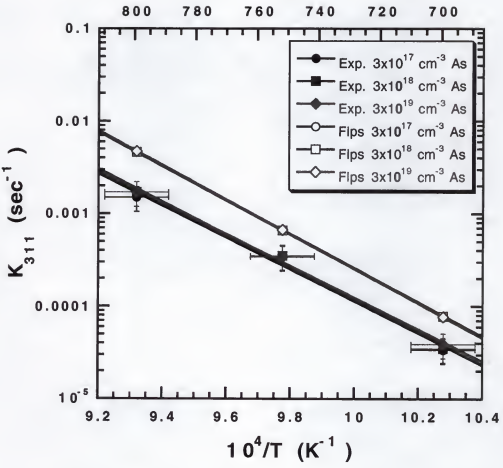

Figure 4.12. Differences in activation energy calculation between the experiment and simulations. The difference in the curves is attributed to both an error in counting and a temperature differential. The simulation predicts a 3.6 eV activation while the experiment produced an energy of 3.4 eV.

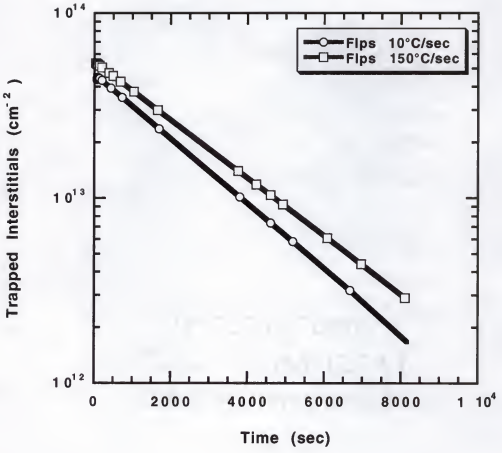

Figure 4.13. Effect of changing the ramp rate in the simulations. A higher ramp rate leaves less time for the As-I pairs to form before the {311} nucleate therefore, there is less dependence on the concentration at zero time.

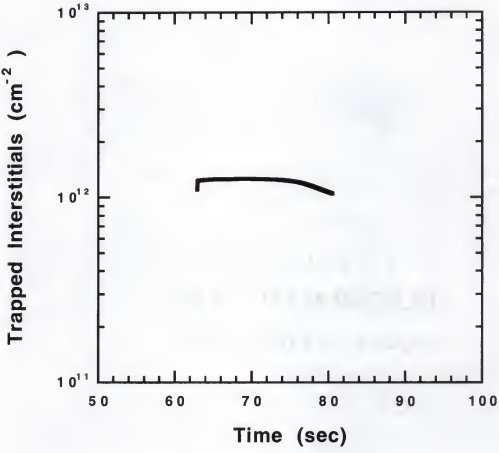

Figure 4.14. Defect formation with no arsenic present in low energy, high dose simulations. When arsenic is present no defects form which is consistent with previous studies.

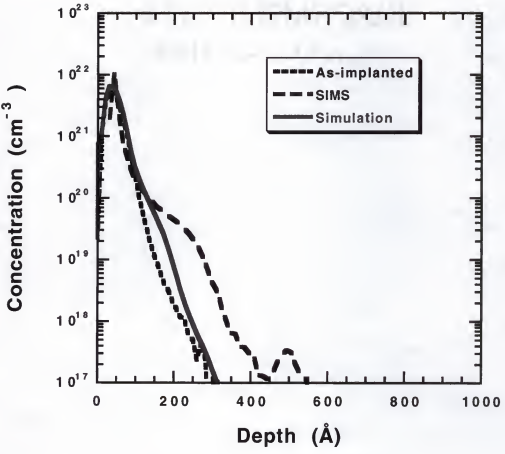

Figure 4.15. Diffusion simulations of 3 keV $1x10^{15}$ cm^{-2} arsenic profiles. When arsenic diffusion simulations neglect diffusion with interstitials, the diffusion is underestimated.

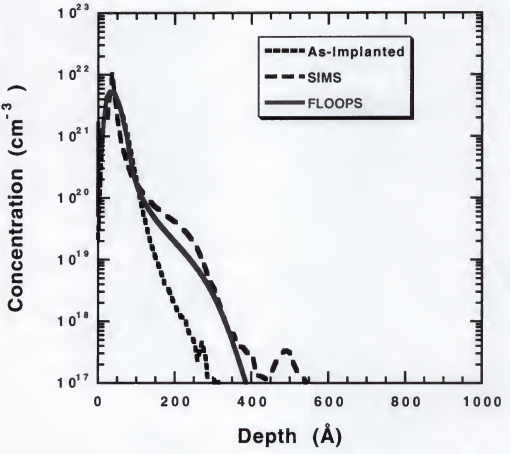

Figure 4.16. Diffusion simulations of 3 keV $1x10^{15}$ cm^{-2} arsenic implants at 800°C for 1 hr. When diffusion by interstitials is accounted for, the simulations better predict the profile motion.

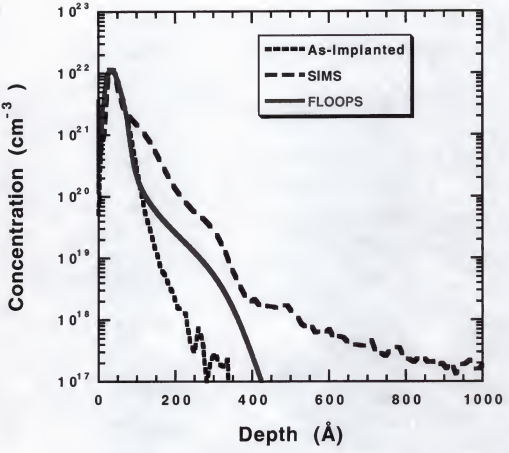

Figure 4.17. Simulation of 3 keV $5x10^{15}$ cm^{-2} arsenic implant annealed at 800°C for 1 hr with As-I diffusion accounted for. The model underestimates the diffusion. This is possibly due to the effects from the clustering and precipitation process that were not accounted for.

CHAPTER 5
SUMMARY AND FUTURE WORK

5.1 Summary

For the optimization of shallow junction devices, the understanding of transient enhanced diffusion (TED) is crucial. The excess interstitials introduced by ion implantation are thought to be the driving force behind TED. In order to control the dopant diffusion and TED in the long term, it is crucial to first understand the dopant-interstitial interactions that lead to enhanced diffusion. This work is directed toward understanding the arsenic-interstitial interaction in silicon. A brief summary is presented hereafter.

The first step was to look at the effect of arsenic on the number of trapped interstitials in {311} defects. {311} defects are known to be made up of silicon interstitials and dissolve through the release of those interstitials. Arsenic wells were formed of varying concentrations and a silicon implant known to cause {311} formation and introduced. It was found that indeed arsenic has an effect on the nucleation of {311} defects. However, once the defects formed there was no effect from

arsenic on the dissolution process. At high enough concentrations no defects formed at all.

From these experiments it is believed that during the early stages of annealing there is a competition between arsenic atoms and {311} defects. At lower temperatures it seems that arsenic-interstitial pairs are favorable due to possibly a lower formation energy. As the temperature continues to increase the energy of formation for a {311} defect is overcome and becomes the favored location for the interstitials. With a number of interstitials already bound up in pairs, the number of nucleated {311}'s is reduced. Therefore as the arsenic concentration increases the number of arsenic available to form pairs increases as well. The same silicon implant was used in all cases so, the same number of interstitials are available at each concentration to be bound. Due to more pair possibilities at higher concentrations, less {311}'s nucleate.

Once the {311} defects formed there was no change in dissolution behavior. A number of dissolution curves were constructed at each temperature and arsenic concentration studied. It was found that in all comparable cases the dissolution rate constant or the slope was equal. This indicates that the defects are all dissolving at the same rate, all be it from a different starting point. This result held true for activation energy calculations also. The dissolution rate constant was found to be 50

±5min and the activation energy for the dissolution was found to be 3.4 ±0.2eV. Both of these values are within the range of published studies for pure {311} experiments.

It is know believed that the controlling factor in the dissolution of {311} defects is the ability of an interstitial to leave the end of the defect. The result that arsenic does not affect the dissolution rate may have two possible explanations. The first is that the amount of interstitials that are given off by the As-I pairs is far less than the amount of interstitials being released by {311} defects. If this is the case then, the interstitials from the pairs have very little to add to the total population of interstitials in the bulk and no effect will be noticed. Possibly a more sensitive technique would pick up the release. A second possibility is that since the interstitial release is mediated at the ends of the defects and the As-I pairs have no effect on the release rate, therefore no effect on the dissolution occurs. The results for arsenic are also consistent with the studies performed on boron and phosphorus. However, since arsenic is a partial vacancy diffuser, boron and phosphorus have a much stronger effect on the nucleation results. The dissolution for {311} defects also does not change under the influence of the other dopants.

It was also shown that the {311}'s that do form have a smaller size distribution at higher arsenic concentrations. As with all growth and dissolution phenomena the larger defects grow at the expense of smaller ones due to a critical size ratio. At higher concentrations the defects were smaller in general so at equal time intervals the defects dissolved faster. For example after 15 minutes at 800°C there are smaller and fewer defects at the higher concentrations compared to lower concentrations.

In order to capture the release of interstitials from arsenic implanted region, boron marker layers studies were devised. Boron is known to be a pure interstitial diffuser and if designed correctly can be used as a detector for interstitials. By placing a boron marker layer below the surface of the silicon, additional implants can be introduced into the wafer and upon annealing the motion of the marker layer can be monitored. Comparisons of implanted and non-implanted wafers leads to differences in interstitial fluxes and therefore in diffusion of the marker layer.

CVD boron marker layers were grown at a depth of 4500Å from the surface. Arsenic was then implanted and RTA annealed to form a well like structure. Subsequent to the arsenic implants, silicon implants were introduced to add excess interstitials. The goal was to monitor the

release of interstitials from the implanted area and see what effect arsenic had. Control wafers were also devised with only arsenic and only silicon.

Comparisons of the control wafers showed that there was no difference in diffusion from the RTA annealing between a no implant wafer and an arsenic implant. In other words, the damage from the arsenic implant had no effect on the motion of the boron spike after RTA. This has been seen in other studies of the same material as well. Lower temperature furnace anneals were done on the wafers to monitor the release.

It was found that arsenic had a small effect on the release of the interstitials from the implanted area. At short times there was a delay in the diffusion enhancement of the boron marker layers. This is consistent to what was seen in the well experiment where the As-I pairs and slows the nucleation of defects. It seems that these pairs also delay the diffusion as well. At longer times at temperature there is increased diffusion from all sources. Unfortunately it was difficult to separate the differences in diffusion from the arsenic and silicon implants. The concentration of arsenic was a little high and it is believed that As_nV formation caused extra interstitials to be injected. In earlier studies it was shown that at higher concentrations arsenic combines with vacancies

and causes an interstitial to be kicked out which to enhanced diffusion of the marker layers. Later results proved this to be true when a lower dose of arsenic was used and no enhanced diffusion was seen from the arsenic only case.

Modeling of the interaction is the most important result to come from this experiment. The long term goal of this work was not only to learn the dopant-interstitial interaction, but also to be able to apply the result, in the form of a model, for future process simulation. To model the arsenic-interstitial interaction a simple approach was taken. Recently a new model was instituted into FLOOPS that predicted the nucleation and dissolution of {311} defects. An arsenic background was added to the model and a simple pair model was used to effect the interstitial population.

The model that was used was of the form, $C_{AsI} = C_I * C_{As} \frac{\exp\left[\frac{E_b}{kT}\right]}{5x10^{22}}$

where C_I is the concentration of interstitials from a UTMARLOWE simulation, C_{As} was the arsenic concentration, E_b is the binding energy, k is Boltzman's constant and T is the temperature in Kelvin. Using this equation a binding energy was chosen between 0 and 1 eV. It was found that with zero interstitial binding energy there was no effect from the arsenic background. With increasing energy more effect was noticed. At

this point the modeled seemed promising for two reasons. One, the difference in nucleated {311} at time zero was decreasing with increasing arsenic concentration and two there was no effect of the arsenic on the dissolution rate. These were both results seen in the experimental portion of this work. It should be noted that there is no formation barrier for the As-I pair and 0.5 eV formation energy for the {311} defects. This allows the arsenic-interstitial interaction to take place at the initial stages of the annealing cycle.

Comparing the effect of different binding energies to that of the data, lead to a best-fit binding energy of ~0.95 eV. This energy seems to be a reasonable energy for this system. The binding energy was tested in a number of different ways and found to best fit all circumstances. It was also determined that there is no effect with temperature and that this energy can be used across all concentrations. The fact that these simulations matched what the experimental data showed was a promising result. At this point the simulations were run for all studied cases and fit well at most concentrations and temperatures. However, at higher concentrations and lower temperatures, which is a worst case scenario when supersaturation is considered, the results begin to vary. It is believed that in the experimental data effects from the arsenic clustering may be beginning to take shape. The present model does not take these

effects into account and a newer, more complicated model needs to be invoked to account for cluster formation. At the present time there is not a continuum model that expands throughout the entire arsenic concentration range. In the experiments the activation energy for the dissolution process was found to be 3.4 eV, while in the simulations a activation energy of 3.6 eV resulted. The difference is accounted for in experimental counting errors and possible temperature deviations in the annealing cycles.

The As-I pair model was applied to low energy, high dose arsenic implants annealed for 1 hr at 800°C. The simulations show that in some cases the enhanced diffusion can be attributed to the interstitials in the end of range. The lack of defects seen by Jones et al.[82] was attributed to the interstitials and the simulations were consistent with that theory. The model lacks the precipitation and clustering effects seen in other experiments and needs to be added to correctly simulate extremely high dose cases.

In conclusion many experiments were done to look at the arsenic-interstitial interaction. It was found that arsenic and interstitials react to form defect pairs in the initial periods of the annealing cycles. The formation of these pairs causes less interstitials to be available for the formation of {311} defects. Once the {311} defects form the arsenic

has no effect on the {311} dissolution process. The amount of interstitials captured by the arsenic atoms is not enough to flood the systems at a longer time when {311}'s are dissolving and therefore there is no effect on the dissolution. A small effect is also seen at the initial stages in boron marker layer experiments. The arsenic-interstitial interaction was modeled with a simple pair model at most concentrations of study. The best fit to the data was found when a binding energy of 0.95 eV was used. Further models need to be incorporated such that the effect of arsenic is captured throughout a larger range of concentrations.

5.2 Future Work

There is still a considerable amount of work that may be completed in this subject area. The following are a few suggestions for future directions.

1. In terms of industrial importance, activation studies need to be carried out. Of utmost importance to the fast growing semiconductor industry is how to increase the electrical activation of source/drain regions. A study of activation/deactivation may lead to a more detailed model of how the arsenic-interstitial interaction is occurring.

2. Higher arsenic concentration studies. This goes along with the activation/deactivation studies. At high enough concentrations, arsenic will deactivate and form precipitates. How this happens may be crucial to understanding how to increase the electrical activation in arsenic implanted regions.
3. Use the effects that were found and transfer them to shallow junction technology. The results may have interesting implications when studying the diffusion of shallow junctions.
4. Build a continuum model that ranges across the entire useful arsenic concentration range. As of now there is no model of such and it would be beneficial to be able to use one model for arsenic no matter what the concentration or anneal condition
5. Presented in the modeling work was an effect of ramp rate on the pair formation. Studies can be done at various ramp rates to test this theory of the pair formation being at the initial stages of annealing in this way.

APPENDIX A
PEAK ADJUST MACRO

A.1 Boron Marker Layer Adjustments

Secondary Ion Mass Spectrometry (SIMS) provides an excellent technique for quantifying dopant profiles. However, when the depth profiles are measured there can be considerable error in the measurements. In the SIMS analysis of the boron spike in Chapter 3, there are several things that are constant. Due to the fact that the samples are all from the same wafer, the depth and dose of the spikes are equal. Due to measurement errors inherent in SIMS analysis these parameters may not always turn out equal from sample to sample. To quickly adjust for any measurement errors an Excel macro was developed.

In the macro the initial curve is fit with a Gaussian curve function. The parameters of a Gaussian curve are the depth of the peak, the peak concentration and the standard deviation. Once the depth of the peak is determined then it is multiplied by the percent difference of a set value. The set value is the value at which the peak should be located. This will move the peak and the rest of the profile equally to the set depth.

When comparing different profiles the area under the curve is also an important value. In these studies it is assumed that no boron is lost to the bulk. In other words, the area under the curve should remain constant throughout the experiment. This function is also adjusted for in the development of the macro. By measuring the area under the curve of the as grown spike the standard value may be set. Similar to the depth correction the dose can also be standardized. By measuring the area under each curve the value may be multiplied by the percent difference between the actual curve and the standard.

By using this macro a number of parameters may be equalized for easier comparisons. The following macro will correct the depth of the peak to a set standard value, correct the dose to a set value, plots the data for quick checks of adjustments and saves the corrected data into a text file. The visual basic script is listed in the next section.

A.2 Peak Adjust Macro

```
Sub Peak_Adjust()
' Macro1 Macro
' Macro recorded 1/25/00 by Rich Brindos

'opens and parses data files
    Dim fileNames As Variant
    Dim peak As Variant
    Dim depth As Variant
    Dim width As Variant
    Dim cordepth As Variant
    Dim cordose As Variant
```

```
    ChDir "Brindos:R. Brindos:SIMS Data:As 5e14 -B Spikes:ASC Data:"
    fileNames = Application.GetOpenFilename()
    Workbooks.OpenText FileName:=fileNames, Origin _
        :=xlMacintosh, StartRow:=4, DataType:=xlFixedWidth,
FieldInfo:=Array( _
        Array(0, 1), Array(7, 1), Array(15, 1), Array(23, 1))
    ActiveSheet.Name = "Sheet1"
'counts the number of data points
    datapoints = 1
    Do While IsEmpty(Cells(datapoints, 1)) = False
    datapoints = datapoints + 1
    Loop

    'MsgBox "Data Points =" & datapoints - 1

'delete first two columns
    Columns("C:D").Select
    Selection.Copy
     Windows("Corrected_Peak_Adjust").Activate
    Range("A1:B1").Select
    ActiveSheet.Paste

'multiply depth by 1e4 to change from microns to angstroms
    Range("C1").Select
    ActiveCell.FormulaR1C1 = "=RC[-2]*1e4"
    Selection.Copy
    Range(Cells(2, 3), Cells(datapoints - 1, 3)).Select
    ActiveSheet.Paste

'Add 1e15 to the Concentration to get rid of zero counts
    Range("D1").Select
    ActiveCell.FormulaR1C1 = "=RC[-2]+1e15"
    Selection.Copy
    Range(Cells(2, 4), Cells(datapoints - 1, 4)).Select
    ActiveSheet.Paste

'name peak, depth, width and lsquare cells
    Range("J1").Select
    ActiveCell.FormulaR1C1 = "Peak"
     ActiveWorkbook.Names.Add Name:="peak", RefersTo:="=R1C11"
```

```
    Range("J2").Select
    ActiveCell.FormulaR1C1 = "Depth"
     ActiveWorkbook.Names.Add Name:="depth", RefersTo:="=!R2C11"
    Range("J3").Select
    ActiveCell.FormulaR1C1 = "Width"
     ActiveWorkbook.Names.Add Name:="width", RefersTo:="=!R3C11"
    Range("J4").Select
    ActiveCell.FormulaR1C1 = "Dose"
     ActiveWorkbook.Names.Add Name:="dose", RefersTo:="=!R4C11"
    Range("J5").Select
    ActiveCell.FormulaR1C1 = "LSquare"
     ActiveWorkbook.Names.Add Name:="lsquare", RefersTo:="=!R5C11"

'set values for initial gaussian
    Range("peak").Select
    ActiveCell.FormulaR1C1 = 1E+18
     Range("depth").Select
    ActiveCell.FormulaR1C1 = 4500
     Range("width").Select
    ActiveCell.FormulaR1C1 = 500

'Adds in gaussian function
    Range("E1").Select
    ActiveCell.FormulaR1C1 = "=(R1C11)*EXP(-((RC[-2]-
(R2C11))^2/(R3C11^2))"
    Selection.Copy
    Range(Cells(2, 5), Cells(datapoints - 1, 5)).Select
    ActiveSheet.Paste

'Adds in Least Squares
    Range("F1").Select
     ActiveCell.FormulaR1C1 = "=(RC[-1]-RC[-2])^2"
    Selection.Copy
    Range(Cells(2, 6), Cells(datapoints - 1, 6)).Select
    ActiveSheet.Paste

'Sums least squares
    Range("lsquare").Select
     ActiveCell.FormulaR1C1 = "=SUM(R[46]C[-5]:R[996]C[-5])"

'Fit gaussian curve to sims data
```

```
    SolverOk SetCell:="Isquare", MaxMinVal:=2, ValueOf:="0",
ByChange:="$K$1:$K$3"
     SolverOptions MaxTime:=100, Iterations:=100, Precision:=0.000001,
AssumeLinear _
       :=False, StepThru:=False, Estimates:=1, Derivatives:=1,
SearchOption:=1, _
        IntTolerance:=0.1, Scaling:=True, Convergence:=0.0001,
AssumeNonNeg:=False

    SolverSolve
 'insert depth and dose to correct to
     cordepth = InputBox("Enter Depth to correct to:")
     Range("L2").Select
     ActiveCell.FormulaR1C1 = cordepth
     cordose = InputBox("Enter correct dose:")
     Range("L4").Select
     ActiveCell.FormulaR1C1 = cordose
     Range("M2").Select
     ActiveCell.FormulaR1C1 = "=RC[-1]/RC[-2]"
     Range("M4").Select
     ActiveCell.FormulaR1C1 = "=RC[-1]/RC[-2]"

'multiply depth by correction factor
     Range("O1").Select
     ActiveCell.FormulaR1C1 = "=RC[-12]*R2C13"
     Selection.Copy
     Range(Cells(2, 15), Cells(datapoints - 1, 15)).Select
     ActiveSheet.Paste

'calculates dose
     Range("G2").Select
      ActiveCell.FormulaR1C1 = "=(RC[8]-R[-1]C[8])*RC[-3]"
     Selection.Copy
     Range(Cells(2, 7), Cells(datapoints - 1, 7)).Select
     ActiveSheet.Paste
     Range("K4").Select
      ActiveCell.FormulaR1C1 = "=(SUM(R[46]C[-4]:R[996]C[-4]))*1E-8"
'multiply dose by correction factor
     Range("P1").Select
     ActiveCell.FormulaR1C1 = "=RC[-12]*R4C13"
     Selection.Copy
```

```
    Range(Cells(2, 16), Cells(datapoints - 1, 16)).Select
    ActiveSheet.Paste

'Adds in gaussian function
    Range("Q1").Select
    ActiveCell.FormulaR1C1 = "=(R4C13*R1C11)*EXP(-((RC[-2]-
(R2C11*R2C13))^2/(R3C11*R2C13)^2))"
    Selection.Copy
    Range(Cells(2, 17), Cells(datapoints - 1, 17)).Select
    ActiveSheet.Paste

'Displays corrected gaussian values
    Range("N1").Select
    ActiveCell.FormulaR1C1 = "=RC[-3]*R4C13"
    Range("N2").Select
    ActiveCell.FormulaR1C1 = "=RC[-3]*R2C13"
    Range("N3").Select
    ActiveCell.FormulaR1C1 = "=RC[-3]*R2C13"
    'Range("N4").Select
    'ActiveCell.FormulaR1C1 = "=RC[-3]*R4C13"

'Dose check for corrected data
    Range("R2").Select
     ActiveCell.FormulaR1C1 = "=(RC[-3]-R[-1]C[-3])*RC[-2]"
    Selection.Copy
    Range(Cells(2, 18), Cells(datapoints - 1, 18)).Select
    ActiveSheet.Paste
    Range("N4").Select
     ActiveCell.FormulaR1C1 = "=(SUM(R[46]C[4]:R[996]C[4]))*1E-8"
End Sub
```

LIST OF REFERENCES

1 M. I. Current, *National Technology Roadmap for Semiconductors*, (Semiconductor Industry Association, San Jose, CA, 1997) p. 188.

2 S. Wolf and R. N. Tauber, *Silicon Processing for the VLSI Era Volume 1-Process Technology*, Vol. 1 (Lattice Press, Sunset Beach, CA, 1986).

3 S. M. Sze, *Physics of Semiconductor Devices* (John Wiley & Sons, New York, NY, 1981).

4 G. F. Cerofolini, P. Manini, L. Meda, G. U. Pignatel, G. Queirolo, A. Garulli, E. Landi, S. Solmi, F. Nava, G. Ottaviani, and M. Gallorini, Thin Solid Films, v 129, n 1-2, p. 111 (1985).

5 G. F. Cerofolini, L. Meda, M. L. Polignano, G. Ottaviani, H. Bender, C. Claeys, A. Armigliato, and S. Solmi, Proceedings - The Electrochemical Society, v 88-4, p. 706 (Electrochemical Soc., Pennington, NJ, 1986).

6 C. M. Hasenack, J. P. De Souza, and J. Erichsen, R., Semiconductor Science and Technology, v 3, n 10, p. 979 (1988).

7 K. S. Jones, S. Prussin, and E. R. Weber, Nuclear Instruments & Methods in Physical Research, Section B: Beam Interactions with Materials and Atoms, v B21, n 2-4, p. 499 (1986).

8 K. S. Jones and S. Prussin, Materials Research Society Symposia Proceedings, v 71, p. 173 (Materials Research Society, Pittsburgh, PA, 1986)

9 R. Kalish, T. O. Sedgwick, S. Mader, and S. Shatas, Appl. Phys. Lett., v 44, n 1, p. 107 (1984).

10 A. Kamgar, F. A. Baiocchi, and T. T. Sheng, Appl. Phys. Lett. v 48, n 16, p. 1090 (1986).

11 S. Mader and A. E. Michel, Phys Status Solidi, v 33, n 2, p. 793 (1976).

12 C. Wagner, A. El-Sadek, and H. J. Mechelke, Phys Status Solidi, v 64, n 1, p. 143 (1981).

13 C. Wagner and A. El-Sadek, Phys Status Solidi A, v 82, n 1, p. 149 (1984).

14 N. D. Young, J. B. Clegg, and E. A. Maydell-Ondrusz, J. Appl. Phys. v 61, n 6, p. 2189 (1987).

15 J. L. Altrip and A. G. R. Evans, Microelectronic Engineering, v 19, n 1-4, p. 367 (1992).

16 V. Krishnamoorthy, D. Venables, K. Moeller, K. S. Jones, and J. Jackson, Defects and Diffusion in Silicon Processing Materials Research Society Proceedings, v 469, p. 401 (Materials Research Society, Warrendale, PA, 1997)

17 D. Venables, V. Krishnamoorthy, H.-J. Gossman, A. Lilak, K. S. Jones, and D. C. Jacobson, Defects and Diffusion in Silicon Processing Materials Research Society Proceedings, v 469, p. 315 (Materials Research Society, Warrendale, PA, 1997)

18 M. Uematsu, J. Appl. Phys. v 82, n 5, p. 2228 (1997).

19 S. Solmi, P. Maccagnani, and R. Canteri, J. Appl. Phys. v 74, n 8, p. 5005 (1993).

20 S. K. Ghandhi, *VLSI Fabrication Principles : Silicon and Gallium Arsenide,* 2nd ed. (John Wiley & Sons, New York, NY, 1983).

21 S. M. Sze, *VLSI Technology*, 2nd ed. (McGraw-Hill, Inc., New York, NY, 1988).

22 J. W. Mayer and S. S. Lau, *Electronic Materials Science: For Integrated Circuits in Si and GaAs* (Macmillan Publishing company, New York, NY, 1990).

23 G. Dearnaley, J. H. Freeman, R. S. Nelson, and S. J., Ion Implantation (North-Holland, Amsterdam, 1973).

24 Y. Xia and C. Tan, Nuclear Instruments & Methods in Physical Research, Section B: Beam Interactions with Materials and Atoms, v 13, n 1-3, p. 100 (1985).

25 J. Lindhard, M. Scharff, and H. Schoitt, Range Concepts and Heavy Ion Ranges, Mat-Fys. Med. K. Dan. Vid. Selsk, v 33, n 14, p. 1 (1963).

26 B. Smith, *Ion Implantation Range Data for Silicon and Germanium Device Technologies*, (Research Studies, Forest Grove, OR, 1977).

27 K. S. Jones, S. Prussin, and E. R. Weber, Applied Physics A: Solids and Surfaces, v A45, n 1, p. 1 (1988).

28 R. B. Fair, J. J. Wortman, and J. Liu, J. Electrochem. Soc., v 131, n 10, p. 2387 (1984).

29 P. M. Fahey, P. B. Griffin, and J. D. Plummer, Reviews of Modern Physics, v 61, n 2, p. 289 (1989).

30 P. A. Stolk, H.-J. Gossmann, D. J. Eaglesham, D. C. Jacobson, and H. S. Luftman, Beam-Solid Interactions for Materials Synthesis and Characterization Materials Research Society Symposium Proceedings, v 354 p. 307 (Materials Research Society, Pittsburgh, PA, 1995).

31 S. J. Pennycook and R. J. Culbertson, Materials Research Society Symposia Proceedings, v 52, p. 37 (Materials Research Society, Pittsburgh, PA, 1986).

32 D. J. Eaglesham, P. A. Stolk, H.-J. Gossmann, T. E. Haynes, and J. M. Poate, Nuclear Instruments & Methods in Physical Research,

Section B: Beam Interactions with Materials and Atoms, v B106, n 1-4, p. 191 (1995).

33 J. F. Ziegler, *Ion Implantation : Science and Technology* (Ion Implantation Technology Co., Edgewater, MD, 2000).

34 C. S. Rafferty, G. H. Gilmer, M. Jaraiz, D. Eaglesham, and H.-J. Gossmann, Appl. Phys. Lett., v 68, n 17, p. 2395 (1996).

35 R. B. Fair, *Rapid Thermal Processing:Science and Technology* (Academic Press, Boston, MA 1993).

36 N. E. B. Cowern, G. Mannino, F. Roozeboom, P. A. Stolk, H. G. A. Huizing, J. G. M. van Berkum, N. N. Toan, and P. H. Woerlee, Advances in Rapid Thermal Processing. Proceedings of the Symposium, v 99-10, p. 125 (Electrochemical Soc., Pennington, NJ, 1986).

37 T. E. Haynes, D. J. Eaglesham, P. A. Stolk, H.-J. Gossmann, D. C. Jacobson, and J. M. Poate, Appl. Phycs. Lett., v 69, n 10, p. 1376 (1996).

38 P. A. Packan and J. D. Plummer, Appl. Phys. Lett., v 56, n 18, p. 1787 (1990).

39 D. J. Eaglesham, P. A. Stolk, J.-J. Gossmann, and J. M. Poate, Appl. Phys. Lett., v 65, n 18, p. 2305 (1994).

40 J. Liu, Ph. D. Thesis, University of Florida, Gainesville, FL, 1996.

41 L. H. Zhang, K. S. Jones, P. H. Chi, and D. S. Simons, Appl. Phys. Lett., v 67, n 14, p. 2025 (1995).

42 N. E. B. Cowern, A. Cacciato, J. S. Cluster, F. W. Saris, and W. Vandervorst, Appl. Phys. Lett., v 68, n 8, p. 1150 (1996).

43 P. H. Keys, J. H. Li, E. Heitman, P. A. Packan, M. E. Law, and K. S. Jones, Si Front-End Processing - Physics and Technology of

Proceedings, v 568, p. 199 (Materials Research Society, Warrendale, PA,1999).

44 R. Brindos, P. Keys, M. E. Law, and K. S. Jones, Appl. Phys. Lett., v 75, n 2, p. 229 (1999).

45 R. Brindos, M. E. Law, K. S. Jones, and E. Andideh, Si Front-End Processing - Physics and Technology of Dopant-Defect interactions. Materials Research Society Symposia - Proceedings, v 568, p. 169 (Materials Research Society, Warrendale, PA,1999).

46 R. Angelucci, G. Celotti, D. Nobili, and S. Solmi, J. Electrochem. Soc. v 132, n 11, p. 2726 (1985).

47 M. A. Berding, A. Sher, M. van Schilfgaarde, P. M. Rousseau, and W. E. Spicer, Appl. Phys. Lett., v 72, n 12, p. 1492 (1998).

48 P. Packan, Ph.D. Dissertation, Stanford University, Palo Alto, CA (1989).

49 P. M. Rousseau, P. B. Griffin, S. C. Kuehne, and J. D. Plummer, Technical Digest - International Electron Devices Meeting, p. 861 (IEEE, Piscataway, NJ, 1994).

50 P. M. Rousseau, P. B. Griffin, W. T. Fang, and J. D. Plummer, J. Appl. Phys., v 84, n 7, p. 3593 (1998).

51 P. M. Rousseau, P. B. Griffin, S. C. Kuehne, and J. D. Plummer, IEEE Transactions on Electron Devices, v 43, n 4, p. 547 (1996).

52 O. Dokumaci, P. Rousseau, S. Luning, V. Krishnamoorthy, K. S. Jones, and M. E. Law, J. Appl. Phys., v 78, n 2, p. 828 (1995).

53 A. Parisini, A. Bourret, A. Armigliato, M. Servidori, S. Solmi, R. Fabbri, J. R. Regnard, and J. L. Allian, J. Appl. Phys., v 67, n 5, p. 2320 (1990).

54 S. N. Hsu and L. J. Chen, Appl. Phys. Lett., v 55, n 22, p. 2304 (1989).

55 S. N. Hsu and L. J. Chen, Nuclear Instruments & Methods in Physical Research, Section B: Beam Interactions with Materials and Atoms, v 55, n 1-4, p. 620 (1991).

56 T. E. Seidel, D. J. Lischner, C. S. Pai, R. V. Knoell, D. M. Maher, and D. C. Jacobson, Nuclear Instruments & Methods in Physical Research, Section B: Beam Interactions with Materials and Atoms, v B7-8, n pt 1, p. 251 (1995).

57 J. L. Hoyt and J. F. Gibbons, Rapid Thermal Processing, Materials Research Society Symposia - Proceedings, v 52, p. 15 (Materials Research Society, Pittsburg, PA,1986).

58 D. Nobili, A. Carabelas, G. Celotti, and S. Solmi, J. Electrochemical Soc., v 130, n 4, p. 922 (1983).

59 A. Armigliato, D. Nobili, S. Solmi, A. Bourret, and P. Werner, J. Electrochemical Soc., v 133, n 12, p. 2560 (1986).

60 N. R. Wu, P. Ling, D. K. Sadana, and J. Washburn, Proceedings of the Symposium on Defects in Silicon, Proceedings of the Electrochemical Society, v 83-9, p. 366 (Electrochemical Soc. Inc, Pennington, NJ, 1983).

61 K. S. Jones, S. Prussin, and E. R. Weber, J. Appl. Phys., v 62, n 10, p. 4114 (1987).

62 D. Nobili, S. Solmi, A. Parsini, M. Derdour, A. Armigliato, and L. Moro, Physical Review B (Condensed Matter), v 49, n 4, p. 2477 (1994).

63 P. M. Rousseau, P. B. Griffin, and J. D. Plummer, Appl. Phys. Lett., v 65, n 5, p. 578 (1994).

64 P. M. Rousseau, P. B. Griffin, S. Luning, and J. D. Plummer, IEEE Transactions on Electron Devices, v 43, n 11, p. 2025 (1996).

65 P. M. Rousseau, S. W. Crowder, P. B. Griffin, and J. D. Plummer, IEEE Electron Device Letters, v18, n 2, p. 42 (1997).

66 R. B. Fair and G. R. Weber, J. Appl. Phys., v 44, n 1, p. 273 (1973).

67 R. B. Fair and J. C. C. Tsai, J. Electrochem. Soc., v 123, n 4, p. 583 (1976).

68 Y.-T. Lin, R. Subrahmanyan, M. Orlowski, and A. R. Sitaram, Rapid Thermal and Integrated Processing II, p. 231 (Materials Research Society, Pittsburgh, PA, 1993).

69 K. C. Pandey, A. Erbil, G. S. Cargill, R. F. Boehme, and D. Vanderbilt, Physical Review Letters, v 61, n 11, p. 1282 (1988).

70 O. Dokumaci, P. M. Rousseau, S. Luning, V. Krishnamoorthy, K. S. Jones, and M. E. Law, J. Appl. Phys., v 78, n 2, p. 828 (1995).

71 O. Dokumaci, M. E. Law, V. Krishnamoorthy, and K. S. Jones, Ion-Solid Interactions for Material Modification and Processing, Materials Research Society Symposium Proceedings, v 396, p. 167 (Materials Research Society, Pittsburgh, PA, 1996).

72 H. Park and M. E. Law, Appl. Phys. Lett., v 58, n 7, p. 732 (1991).

73 L. C. Kimerling, M. T. Asom, J. L. Benton, P. J. Drevinsky, and C. E. Caefer, Mater. Sci. Forum, v 38, p. 1215 (1993).

74 J. Zhu, Defects and Diffusion in Silicon Processing, Materials Research Society Symposium Proceedings, v 469, p. 151 (1997).

75 S. Thompson, P. Packan, and M. Bohr, Intel Tech. Jour., v Q3, p. 1 (Portland, OR, 1998).

76 R. Raman, M. E. Law, V. Krishnamoorthy, and K. S. Jones, Appl. Phys. Lett., v 74, n 5, p. 700 (1999).

77 M. I. Current and C. B. Yarling, *Materials and Process Characterization of Ion Implantation*, 1st ed., p. 223 (Ion Beam Press, Austin, TX, 1997).

78 J. Desroches, V. Krishnamoorthy, K. S. Jones, and C. Jasper, Defects and Diffusion in Silicon Processing, Materials Research Society Symposium Proceedings, v 469, p. 283 (1997).

79 K. Moller, K. S. Jones, and M. E. Law, Appl. Phys. Lett., v 72, n 20, p. 2547 (1998).

80 G. P. Barbuscia, G. Chin, R. W. Dutton, T. Alvarez, and L. Arledge, Technical Digest - International Electron Devices Meeting 1984, p. 757 (IEEE, New York, NY, 1984).

81 A. Armigliato and A. Parisini, J. Mater. Res., v 6, n 8, p. 1701 (1991).

82 K. S. Jones, D. Downey, H. Miller, J. Chow, J. Chen, M. Puga-Lambers, K. Moller, M. Wright, E. Heitman, J. Glassberg, M. E. Law, L. Robertson, and R. Brindos, Proceedings of the International Conference on Ion Implantation Technology, v 2, p. 841 (IEEE, Piscataway, NJ, 1998).

83 A. Armigliato, A. Parisini, M. Derdour, P. Lazzari, L. Moro, D. Nobili, S. Solmi, Gettering and Defect Engineering in Semiconductor Technology Proceedings, 4 Int Autumn Meet Gettering Defect Eng Semicond Technol GADEST 1991, p. 393 (Trans Tech Publ, Zuerich, Switz., 1991).

84 A. Armigliato, A. Parisini, M. Derdour, P. Lazzari, L. Moro, D. Nobili, and S. Solmi, Diffus. Defect Data, Solid State Data B, Solid State Phenom. (Liechtenstein), Diffusion and Defect Data - Solid State Data, Part B (Solid State Phenomena), v 19-20, p. 393 (1991).

85 A. Parisini, D. Nobili, A. Armigliato, M. Derdour, L. Moro, and S. Solmi, Applied Physics A (Solids and Surfaces), v A54, n 3, p. 221 (1992).

86 M. Ramamoorthy and S. T. Pantelides, Physical Review Letters, v 76, n 25, p. 4753 (1996).

87 S. Solmi and D. Nobili, J. Appl. Phys., v 83, n 5, p. 2484 (1998).

88 H. J. Gossmann, F. C. Unterwald, and H. S. Luftman, Journal of Applied Physics, v 73, n 12, p. 8237 (1993).

89 H.-J. Gossmann, A. M. Vredenberg, C. S. Rafferty, H. S. Luftman, F. C. Unterwald, D. C. Jacobson, T. Boone, and J. M. Poate, J. Appl. Phys., v 74, n 5, p. 3150 (1993).

90 M. Derdour, D. Nobili, and S. Solmi, J. Electrochemical Soc., v 138, n 3, p. 857 (1991).

91 M. Uematsu, Jpn. J. Appl. Phys., v 39, n 3A, p. 1006 (2000).

92 D. J. Eaglesham, T. E. Haynes, H.-J. Gossman, D. C. Jacobson, P. A. Stolk, and J. M. Poate, Appl. Phys. Lett., v 70, n 24, p. 3281 (1997).

93 G. Lulli, M. Bianconi, S. Solmi, E. Napolitani, and A. Carnera, J. Appl. Phys., v 87, n 12, p. 8461 (2000).

94 Law, M. E., FLOODS/FLOOPS User Manual, Gainesville, FL (2000).

95 A. Agarwal, H.-J. Gossman, D. J. Eaglesham, L. Pelaz, D. C. Jacobson, J. M. Poate, and T. E. Haynes, Mater. Sci. Eng. A, Struct. Mater., Prop. Microstruct. Process. (Switzerland), Materials Science & Engineering A (Structural Materials: Properties, Microstructure and Processing), v A253, n 1-2, p. 269 (1998).

96 A. D. Lilak, S. K. Earles, M. E. Law, and K. S. Jones, Appl. Phy. Lett., v 74, n 14, p. 2038 (1999).

97 H. Saleh, MS Thesis, University of Florida, Gainesville, FL (2000).

98 J. Nelson, Private Communication (2001).

99 O. Sugino and A. Oshiyama, Solid State Physics, v 27, n 7, p. 1 (1992).

100 C. S. Nichols, Physical Review B (Condensed Matter), v 40, n 8, p. 5484 (1989).

BIOGRAPHICAL SKETCH

The author was born on July 28, 1971, in San Jose, California. After high school, he attended San Jose State University (SJSU) and completed a Bachelor of Science degree in Materials Science and Engineering. Soon after graduating from SJSU the author traveled to the University of Florida (UF) to begin his Masters and Ph.D. studies. Two years later the Masters degree was completed and Ph.D. work followed. The next three years were spent completing the Ph.D. under the advisement of Dr. Kevin S. Jones. The Ph.D. was completed in May 2001.

I certify that I have read this study and that in my opinion it conforms to acceptable standards of scholarly presentation and is fully adequate, in scope and quality, as a thesis for the degree of Doctor of Philosophy.

Kevin S. Jones, Chairman
Professor of Materials Science & Engineering

I certify that I have read this study and that in my opinion it conforms to acceptable standards of scholarly presentation and is fully adequate, in scope and quality, as a thesis for the degree of Doctor of Philosophy.

Mark E. Law
Professor of Electrical and Computer Engineering

I certify that I have read this study and that in my opinion it conforms to acceptable standards of scholarly presentation and is fully adequate, in scope and quality, as a thesis for the degree of Doctor of Philosophy.

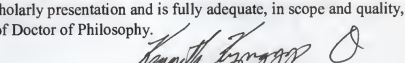

Kenneth O
Professor of Electrical and Computer Engineering

I certify that I have read this study and that in my opinion it conforms to acceptable standards of scholarly presentation and is fully adequate, in scope and quality, as a thesis for the degree of Doctor of Philosophy.

Paul Holloway
Professor of Materials Science & Engineering

I certify that I have read this study and that in my opinion it conforms to acceptable standards of scholarly presentation and is fully adequate, in scope and quality, as a thesis for the degree of Doctor of Philosophy.

Cammy R. Abernathy
Professor of Materials Science & Engineering

I certify that I have read this study and that in my opinion it conforms to acceptable standards of scholarly presentation and is fully adequate, in scope and quality, as a thesis for the degree of Doctor of Philosophy.

Fred Stevie
Member of Technical Staff,
Agere Systems

This thesis was submitted to the Graduate Faculty of the College of Engineering and to the Graduate School and was accepted as partial fulfillment of the requirements for the degree of Doctor of Philosophy.

May 2001

M. Jack Ohanian, Interim Dean
College of Engineering

Winfred M. Phillips, Dean
Graduate School